Incongruent chemical weathering and adsorption of neodymium drive modulation of neodymium isotope composition of global riverine particulate matter

Anup Kumar Sharma[1*], Tarun Kumar Dalai[1*], Prem Chand Kisku[2], Jitendra Kumar Pattanaik[3], Sambuddha Misra[4], Shivansh Verma[5], Anil Dutt Shukla[5,6]

[1]Department of Earth Sciences, Indian Institute of Science Education and Research Kolkata, Mohanpur 741246, India

[2]Council of Scientific and Industrial Research-National Geophysical Research Institute (CSIR-NGRI), Uppal Road, Hyderabad 500007, India

[3]Department of Geology, Central University of Punjab, Bathinda, Punjab 151401, India

[4]Centre for Earth Sciences, Indian Institute of Science, Bangalore 560012, India

[5]Geosciences Division, Physical Research Laboratory, Ahmedabad 380009, India

[6]Department of Geology, HNB Garhwal University, Srinagar, Uttarakhand 246174, India

*Authors for correspondence: (aks18rs032@iiserkol.ac.in, dalai@iiserkol.ac.in)

Abstract

We report incongruent weathering and differential release of radiogenic neodymium (^{143}Nd) to challenge the widely accepted congruent behaviour of Nd isotopes during weathering of rocks. Investigating two basaltic weathering profiles of the Rajmahal Volcanic Province in India, the incongruent behaviour of minerals and Nd isotopes were established. These results contradict the premise of invariant nature of $^{143}Nd/^{144}Nd$ (expressed as ε_{Nd}) during surface processes, the basis for extensive application of ε_{Nd} in geological and geochemical studies. We also demonstrate that the ε_{Nd} of Nd released to the weathering solution is reliably captured by the oxyhydroxide phases of the weathering profiles. Combining these two observations, we hypothesize that riverine particulate ε_{Nd} is sensitive to adsorption of dissolved Nd and would be regulated by the duration of water-particle interaction during transport. Therefore, we predict that particulate ε_{Nd} would be different between the high and low discharge periods in a river catchment.

Utilising published results of fourteen rivers from across the world, which cover multiple lithologies and climatic regimes, we demonstrate that differential release of Nd isotopes via incongruent weathering and Nd adsorption collectively modulate particulate ε_{Nd} through the length and duration of river transport. An important implication of this study is that the ε_{Nd} offset between the leachates and detrital phases of marine sediments can be a robust tracer for investigating continental weathering and transport during glacial-interglacial periods.

Keywords

Basalt weathering; Rajmahal Volcanics; adsorption; incongruent behaviour of Neodymium isotopes, riverine transport, water-particle interaction

1. Introduction

Radiogenic neodymium isotope composition ($^{143}Nd/^{144}Nd$, expressed as ε_{Nd}, Goldstein and Jacobsen, 1987) has wide applications in investigating crustal extraction and evolution, determining continental weathering fluxes and sediment sources, and tracing ocean water masses. ^{143}Nd is a α-decay product of ^{147}Sm ($t_{1/2}$ = 106 Byr). Therefore, the ε_{Nd} value of an igneous or metaigneous rock is governed by its age and Sm/Nd ratio whereas the composition of the primary source rocks regulates ε_{Nd} of a sedimentary or metasedimentary rock. An implicit requirement for unbiased application of ε_{Nd} is the congruent behavior of Nd isotopes during weathering, i.e., ε_{Nd} of the parent rock, dissolved phase (river water) and the weathering product (sediments) should be identical. The underlying basis for congruent behaviour of Nd isotopes is the knowledge that after its initial release during weathering, Nd is dominantly transported in the solid phase(s) (Piepgras et al., 1979; Elderfield and Greaves, 1982; Goldstein et al., 1984). Insignificant, yet quantifiable difference between ε_{Nd} of source rock and river water, and between river water and suspended particulate matter (SPM) were alluded to by early investigations (Goldstein and Jacobsen, 1987). However, several studies have clearly documented the difference between ε_{Nd} of parent rocks and the weathered products (Martin et al., 1999; Ohlander et al., 2000; Aubert et al., 2001; Ma et al., 2010; Babechuk et al., 2015; Banerjee and Chakrabarti, 2016; Horbe et al., 2022); between source rocks and river/ground water (Andersson et al., 2001; Aubert et al., 2001; Negrel et al., 2001; Viers and Wasserburg, 2004; Leybourne and Cousens, 2005; Wallrich et al., 2020); between river water and SPM (Henry et al., 1996; Aubert et al., 2001; Rickli et al., 2013; Chatterjee and Singh, 2014; Merschel et al., 2017; Hindshaw et al., 2018); between source rocks and SPM (Martin et al., 1999; Aubert et al., 2001); and between leachable and detrital phases of sediments (Tricca et al., 1999; Adebayo et al., 2018; Sufke et al., 2019; Jang et al., 2020; Larkin et al., 2021). These studies document incongruent behaviour of Nd

isotopes driven by incongruent weathering in catchments comprising of igneous, sedimentary, and mixed lithologies. Therefore, incongruent behaviour of Nd isotopes during weathering is prevalent across the globe, irrespective of the lithology of the catchment. The unraveling of the incongruent behavior of Nd isotopes during weathering was possible due to advancement in instrumentation which allowed for more precise ε_{Nd} determination, with uncertainties of up to ±0.3 (Viers et al., 2008; Rousseau et al., 2019; Moquet et al., 2020) compared to up to ±0.9 in earlier studies (Goldstein and Jacobsen, 1987; Goldstein and Jacobsen, 1988).

Multiple mechanisms have been put forward for explaining the incongruent behaviour of Nd isotopes. These include: (i) differential mineral weathering (Andersson et al., 2001; Aubert et al., 2001; Ohlander et al., 2000; Viers and Wasserburg, 2004; Leybourne and Cousens, 2005; Chatterjee and Singh, 2014; Dausmann et al., 2019; Sufke et al., 2019; Wallrich et al., 2020); (ii) preferential release of more labile phases of Nd (Goldstein and Jacobsen, 1987; Hindshaw et al., 2018; Jang et al., 2020; Horbe et al., 2022); and (iii) disproportionate contributions from different lithologies to riverine SPM (Henry et al., 1996; Chatterjee and Singh, 2014; Merschel et al., 2017) and surface sediments (Bouchez et al., 2011; Garcon and Chauvel, 2014; Bayon et al., 2015; Bayon et al., 2020a). The incongruent behaviour and release of radiogenic Nd isotopes discussed in this study could arise due to any one or a combination of the processes mentioned above, and should not be misconstrued with Nd isotope fractionation.

Weathering profiles of granitic to granodioritic rocks, sedimentary rocks, and coal bearing units unequivocally document incongruent behaviour of Nd isotopes (Aubert et al., 2001; Negrel et al., 2001; Viers and Wasserburg, 2004; Ohlander et al., 2000; Wallrich et al., 2020; Horbe et al., 2022). During basalt weathering, however, there is significant ambiguity on behaviour of Nd isotopes given that both congruent (Martin et al., 1999; Nobre Silva et al., 2010) and incongruent (preferential release of

91 radiogenic Nd, Ma et al., 2010) release of Nd isotopes is reported. Additional data on Nd isotopes in
92 basaltic weathering profiles is required for a clear assessment of congruent vs. incongruent behaviour of
93 Nd isotopes during basalt weathering. In this study, this gap in knowledge is filled by quantifying the
94 trends and aberrations in Nd isotopes in the bulk rocks, weathered products and adsorbed
95 (oxyhydroxides) phases of two weathering profiles developed on basaltic rocks of the Rajmahal
96 Volcanics Province (RVP) in India (Supplementary Note SN1). Our study provides clear evidence of
97 incongruent behavior of Nd isotopes during weathering and capture of Nd isotope composition of
98 weathering solutions in the oxyhydroxide phases. Furthermore, utilizing the published data for fourteen
99 global rivers, we demonstrate that incongruent behaviour of Nd isotopes during weathering and
100 adsorption of dissolved Nd riverine transport influence the particulate ε_{Nd} composition at a global scale.

101 ## 2. Material and methods

102 Two weathering profiles developed on the basaltic rocks of the RVP (Supplementary Note SN1)
103 were chosen after careful evaluation of their state of preservation and external contamination by aeolian
104 inputs (Supplementary Note SN2 and Fig SF3). Dried samples of basaltic parent rocks and their
105 weathered materials collected from the profiles were weighed in pre-cleaned quartz crucibles and
106 combusted at 550°C in a muffle furnace for ~5 hours to oxidize the organic matter. About 100 mg of
107 ashed samples and reference standards were accurately weighed in a pre-cleaned PFA vial (Savillex®).
108 To these vials, we added an acid mixture containing 3 mL of HCl and 1 mL of HNO_3 (both double-
109 distilled on PFA stills from concentrated analytical grade acids), and 2 mL of ultrapure concentrated HF.
110 The acid-sample mixture was quantitatively digested at 160°C for ~72 hours. The vials were opened
111 after they cooled to room temperature. All operation was conducted under clean workbench conditions
112 (Class-100) and the solutions were dried under identical environment. Subsequently, a few mL of HNO_3

was added to the residue for dissolution, followed by evaporation to drive-off residuary HF. The digested samples were redissolved in ~60 g of 5% HNO_3. These solutions were analyzed by ICPMS. The procedural blanks and sample replicates were processed in every batch of digestion. The HNO_3 and HCl used for sample processing were double-distilled (DD) in a Savillex® DST-1000 sub-boiling distillation system and the ultrapure grade HF was commercially procured.

For measurements on X-Ray spectrometer (XRF), fusion beads were made. In brief, the powdered samples were accurately weighed and mixed with a flux of 65% lithium tetraborate and 35% lithium metaborate in a 1:10 ratio. After thorough mixing, a few grains of lithium bromide were added to the mixture. These mixtures were quantitatively transferred into platinum crucibles and melted at 1250 ºC. The melted mixtures were poured into pre-heated platinum moulds to form the fusion beads of required shape and size.

Selective extraction of the exchangeable and amorphous Fe-Mn oxyhydroxides phases was carried out by a two-step leaching procedure (Gupta and Chen, 1975; Chen et al., 2012). For exchangeable fractions, ~ 3 g of powdered sample was added to a pre-cleaned 50 mL centrifuge tube and leached with 40 mL of 1N ammonium acetate (Sigma Aldrich, > 99.99% purity) buffered at pH 7 with superpure ammonium hydroxide. These mixtures were kept overnight on a reciprocating shaker at 400 rpm and finally centrifuged at 5000 rpm. The supernatant fractions were decanted into precleaned PFA beakers. The residues were washed three times with Milli-Q water (18.2 MΩ) and washings were collected and mixed with the supernatant. These solutions were dried and redissolved in 5% HNO_3 for elemental analysis and another aliquot in 2N HCl for chromatographic purification required for Nd isotopic analysis. To extract the oxyhydroxides phases, a mixture of 40 mL 0.005 N hydroxylamine hydrochloride (HH; 99.999% purity), 1.5% acetic acid (≥99.99% purity) and 0.03 N

135 ethylenediaminetetraacetic acid (EDTA; 99.995% purity), buffered to pH 4 with sodium hydroxide, was
136 added to the residues left after extraction of exchangeable phase. These sample-reagent mixtures were
137 kept for one hour on a reciprocating shaker at 400 rpm. Thereafter, the procedure followed was the same
138 as outlined above for extraction of exchangeable fractions.

139 **2.1. Analysis of major and trace element composition**

140 The fusion beads were analyzed to measure the major element concentrations using a Bruker® Tiger
141 S-8 WD-X-Ray Spectrometer. The accuracy of the measurements was evaluated by analysis of certified
142 reference standards NIST 2711A (Montana II Soil), SDC-1 (Mica Schist) and MESS-3 (Marine
143 Sediment). The measurement accuracies were better than ±8%. The analytical reproducibility, based on
144 replicate analyses of the same sample, was within ±5%.

145 Trace element concentrations were measured by a QQQ-ICP-MS (Agilent® 8900 at IISc, Bangalore)
146 following multi-element external calibration and internal standard addition. Certified reference standards
147 BCR-2 (Columbia River Basalt), BHVO-2 (Hawaiian Basalt) and GSP-2 (Granodiorite) were analyzed
148 to determine the measurement accuracy, which was 5% or better for La, Sm, Th, Sc and Nb and better
149 than 9% for Nd. The analytical reproducibility, evaluated by replicate analyses, was within ±2% for
150 trace elements.

151 The major and trace element concentrations in the exchangeable and oxyhydroxide fractions were
152 measured by a quadrupole ICP-MS (Thermoscientific® X Series 2) at IISER Kolkata. Based on the
153 analysis of certified reference standard BHVO-2 and NIST-traceable standards IV-Stock 26 and IV-
154 Stock 8 (Inorganic Ventures®), the measurement accuracy was better than 3% for Mn and 10% for Nd.

Based on replicate analyses, analytical reproducibility of Mn and Nd are within ±7% for exchangeable and oxyhydroxide phases.

2.2. Purification of Nd and measurement of Nd isotope composition

2.2.1. Bulk samples of weathering profiles

Nd separation from the samples followed a modified method of Lei et al. (2019). The REEs were separated in a two-step cation exchange column chromatography. The first column was loaded with 0.8 mL of AG50W-X8 resin, washed with 6N HCl, 3N HNO_3 and Milli-Q and pre conditioned with 2N HCl. The sample solution was loaded in 2N HCl medium and was eluted with 2N HCl and 2.5N HNO_3 to remove the major elements. The REE fractions were collected in 7N HNO_3, dried and redissolved in 0.15N HCl. The second column was loaded with 1 mL of Ln Spec resin, washed with 6N HCl and Milli-Q and preconditioned with 0.15N HCl. The separated REE fractions from the first column were dried down and then loaded in 0.15N HCl medium and eluted with 0.15N HCl to remove Ba. The Nd fractions were collected in 0.25N HCl and the column was eluted with 6N HCl to remove Sm. The Nd isotope measurements were carried out by a MC-ICP-MS (Thermoscientific® Neptune Plus) facility at IISER Kolkata. Mass bias correction was done by normalizing the measured $^{143}Nd/^{144}Nd$ ratios with a $^{146}Nd/^{144}Nd$ ratio of 0.7219. Analysis of the USGS standard BCR-2 yielded a $^{143}Nd/^{144}Nd$ ratio = 0.512630±0.000002 (2σ, n=2), which agreed well with the reported value of 0.512637±000017 (Weis et al., 2006). The mean external reproducibility of the measured $^{143}Nd/^{144}Nd$ ratio evaluated by replicate sample analyses is ±0.000009 (2σ, n=4).

2.2.2. Oxyhydroxide phases

The Nd concentrations in the oxyhydroxides phases ($[Nd]_{oxy}$) were significantly higher than those in the exchangeable phases ($[Nd]_{exch}$), with $[Nd]_{oxy}/[Nd]_{exch}$ ratios (Supplementary Table ST3) as high as 18

in the Dalahi profile (mean: 8) and 63 in Pakuria profile (mean: 18). Such results clearly indicate that the oxyhydroxides phases are the dominant carrier of adsorbed Nd. Therefore, Nd separation and Nd isotope measurements were carried out only for the oxyhydroxide phases. Our observation of oxyhydroxide phases as the dominant carrier of the adsorbed Nd is in line with the published results (Adebayo et al., 2018; Larkin et al., 2021).

The REEs were separated using a column calibration that is slightly different than that described above for the bulk phases. The columns were loaded with ~2 mL of AG50W-X8 resin, washed with 6N HCl and Milli-Q and conditioned with 2N HCl. The sample solution was loaded in 2N HCl on the preconditioned column and was washed with 2N HCl and 6N HCl. The REE fractions were eluted in 6N HCl. Hereafter, the purification of Nd from REE fractions followed the procedure as outlined above for the bulk phases. The Nd isotope measurements were carried out by a MC-ICP-MS (Thermoscientific® Neptune Plus) facility at the Physical Research Laboratory (PRL), Ahmedabad. Mass bias correction followed a normalization scheme with a $^{146}Nd/^{144}Nd$ ratio of 0.7219. The standard JNdi-1 was measured to evaluate the instrumental stability and yielded an average value of $^{143}Nd/^{144}Nd = 0.512114\pm0.000017$ (2σ, n=11), consistent with the published value of $^{143}Nd/^{144}Nd = 0.512115\pm0.000007$ (Tanaka et al., 2000). Measured $^{143}Nd/^{144}Nd$ ratios for the reference standards were, 0.512637±0.000013 (2σ, n=3) for BCR-2 and 0.512984±0.000015 (2σ, n=7) for BHVO-2, which were in agreement with the reported values of 0.512637±000017 and 0.512987±000010, respectively (Weis et al., 2006). Analysis of four procedural replicate samples provides the mean external reproducibility of the measured $^{143}Nd/^{144}Nd$ ratio to be ±0.000005 (2σ, n=4).

3. Results and discussion

3.1. Incongruent behaviour of radiogenic Nd during chemical weathering

The chronology of the RVP basalts is well constrained (118±2 Myr, Baksi, 2022). Prior to isotopic analysis of the weathering profiles, their state of preservation was verified based on elemental composition (Supplementary Note SN2). The compositions of these profiles (Supplementary Table ST1) demonstrate progressive chemical weathering, as evident from drop in [Na], [Ca], [Mg], Si/Al, and increase of [Al] and chemical index of alteration (CIA) towards the surface (Fig. 1). The Nd/Al, Mn/Al and Fe/Al demonstrate upward increasing trends (Fig. 1), suggestive of Nd adsorption onto the secondary phases, specifically the Fe-Mn oxyhydroxides. The incongruent release of radiogenic Nd is unequivocal and can be observed in the upwardly decreasing trend of ε_{Nd} (Fig. 1) and a strong inverse correlation between CIA and ε_{Nd} (Fig. 2a). These observations, together with the significant inverse correlation of Sm/Nd ratio with CIA (Fig. 2b), underscore preferential weathering of minerals that have higher Sm/Nd (Aubert et al., 2001; Negrel, 2006; Garzanti et al., 2011; Garcon et al., 2014; Dausmann et al., 2019) and a more radiogenic ε_{Nd} composition compared to the parent rock (host basalt). Preferential weathering of pyroxenes relative to feldspars was inferred from the composition of rivers draining these RVP basalts in the study area (Kisku et al., 2020). Our inference of preferential weathering of minerals with higher Sm/Nd ratio is consistent with multiple published works on basalt weathering (Martin et al., 1999; Ma et al., 2010; Liu et al., 2013; Babechuk et al., 2014).

The fraction of Nd released from parent basalts during weathering was quantified by normalizing its concentrations with the immobile element Th, which is used to correct for variation in Nd abundance due to mass loss and/or addition. This approach (Supplementary Note SN3) indicates that up to 40 % Nd is lost from the parent basalts during chemical weathering. The ε_{Nd} of the residual phases post weathering was quantified by mass balance considerations of the [Nd] and ε_{Nd} signatures of bulk materials and

adsorbed (oxyhydroxide) phases (see Supplementary Note SN4, Supplementary Table ST3). We observe that the ε_{Nd} values of the residual phases are lower by up to 0.94 units compared to the bulk materials. Furthermore, the ε_{Nd} values of the bulk materials in the weathering profiles are primarily modulated by the residual phases since they account for a major fraction of Nd (74 % to 98 %, Supplementary Table ST3).

A measure of radiogenic Nd released to the weathering solutions can be assessed from the differences of ε_{Nd} between the parent rock and residual phases ($\Delta\varepsilon_{Nd}^{P\text{-}Res}$). The $\Delta\varepsilon_{Nd}^{P\text{-}Res}$ is characterized by a downward decreasing trend and exhibits a strong positive correlation with CIA (Fig. 3, Supplementary Table ST3). This indicates that the degree of release of radiogenic Nd to the weathering fluid scales with degree of chemical weathering. The importance of solid-solution interaction of major cations in river catchments has been previously recognized (Clow and Mast, 2010; Tipper et al., 2021) It has been widely reported that Nd is highly susceptible to water-particle interactions, whereby dissolved Nd is adsorbed onto the solid phases, specifically the Fe-Mn oxyhydroxides (Fee et al., 1992; Steinmann and Stille, 2008; Ma et al., 2007; Liu et al., 2019; Bai et al., 2023). In both the weathering profiles we observe a strong positive correlation between $\Delta\varepsilon_{Nd}^{P\text{-}Res}$ vs. $\frac{[Mn]_{ox}}{[Mn]_{bulk}}$ (Fig. 4), where ox and bulk refer to the oxyhydroxide (chemically extracted) and bulk phases, respectively. This observation supports the hypothesis that the Mn oxyhydroxide phases faithfully record the Nd isotope signature (ε_{Nd}) of the weathering solution via adsorption. The present observation of Mn oxyhydroxides being the dominant adsorbent of Nd isotopes from the weathering solution is consistent with the earlier reports that oxyhydroxides are a major carrier of LREEs in the weathering profiles developed on basaltic substrates (Ma et al., 2007; Bai et al., 2023). Our results and published body of work (Larkin et al., 2021; Bayon et

al., 2020b) lend support to the idea that ε_{Nd} of Fe-Mn oxyhydroxide phases can be used as a proxy for hydrogenous ε_{Nd} in freshwater environments.

3.2. A hypothesis for modulation of particulate ε_{Nd} via river transport at a global scale

Many studies have documented pervasive adsorption of dissolved Nd onto the SPM during riverine transport (Elderfield et al., 1990; Sholkovitz, 1995; Shiller, 2002; Steinmann and Stille, 2008; Smith and Liu, 2018). In aquatic systems, the LREEs are preferentially removed from dissolved phase onto Fe-Mn oxyhydroxides (Elderfield et al., 1990; Fee et al., 1992; Sholkovitz, 1995; Shiller, 2002; Steinmann and Stille, 2008; Liu et al., 2019). In addition, organic colloids play a significant role in transporting the REEs and facilitating their removal from solution (Land et al., 1999; Ingri et al., 2000; Dang et al., 2023).

We contend that adsorption of dissolved Nd in rivers is globally significant because the residence time of water and SPM in river catchments, varying from a few days to years (Wallbrink et al., 1998; Ciffroy et al., 2003; McGuire and McDonnell, 2006; Sprenger et al., 2019), are orders of magnitude higher than the experimentally determined kinetics of adsorption of REEs in aqueous medium (Davranche et al., 2005; Ashour et al., 2017; Mosai et al., 2019; Briao et al., 2021). Furthermore, significant abundances of adsorbents, particularly the clay minerals and Fe-Mn oxyhydroxides, in the riverine SPM (Land et al., 1999; Ingri et al., 2000; Steinmann and Stille, 2008) provide the sites for adsorption of dissolved Nd.

In addition to ubiquitous and unequivocal reports of adsorption of dissolved Nd in rivers, majority of studies, including ours, document preferential release of radiogenic Nd via incongruent chemical weathering (Aubert et al., 2001; Negrel et al., 2001; Viers and Wasserburg, 2004; Ma et al.,

2010; Dausmann et al., 2019). This is consistent with dissolved Nd being more radiogenic (higher ε_{Nd}) than the SPM or the source rocks (Henry et al., 1996; Aubert et al., 2001; Rickli et al., 2013; Chatterjee and Singh, 2014; Merschel et al., 2017; Hindshaw et al., 2018). Higher ε_{Nd} is also observed in SPM bound leachable phases compared to the residual/detrital phases in rivers (Tricca et al., 1999; Adebayo et al., 2018; Larkin et al., 2021), fjords (Jang et al., 2020), lakes (Sufke et al., 2019), and oceans (Tachikawa et al., 2004; Chen et al., 2012; Wilson et al., 2013). Preferential weathering of easily weatherable (less weathering resistant) phases, which are characterized by higher Sm/Nd and therefore elevated ε_{Nd} than their host/bulk rocks, has been put forward as a plausible explanation (Aubert et al., 2001; Garzanti et al., 2011; Chatterjee and Singh, 2014; Garcon et al., 2014; Dausmann et al., 2019) for more radiogenic Nd in the leachable phases. However, a few studies also indicate preferential release of unradiogenic Nd over its radiogenic counterpart during weathering (Andersson et al., 2001; Ohlander et al., 2000), which results in dissolved Nd to be less radiogenic than the source rock(s) or SPM (Goldstein and Jacobsen, 1987; Spencer et al., 1995; Andersson et al., 2001). The preferential supply of unradiogenic Nd can either result from its incongruent release during weathering of the source rocks or due to external inputs. It is noteworthy that the explanations put forward by studies documenting enrichment of unradiogenic Nd in the fluid phase do not always indicate its preferential release. For instance, the sole study that suggested preferential loss of unradiogenic Nd during weathering (Ohlander et al., 2000), also recognized the involvement of external sources, namely the impact of dust borne Nd supply. Therefore, the evidence in favour of preferential release of unradiogenic Nd via incongruent weathering remains tenuous.

The growing body of studies, including this one, documenting incongruent behaviour of Nd isotopes together with ubiquitous evidence of Nd adsorption in rivers lead us to posit that the particulate

285 ε_{Nd} would be modulated via solid-solution interaction during riverine transport. We hypothesise that the
286 degree of Nd adsorption is dominantly a function of water-particle interaction time in the catchment area
287 and the streams, which is primarily regulated by water discharge (Anderson et al., 1997; Land et al.,
288 1999; Hindshaw et al., 2019; Liu-Lu et al., 2022). Published studies clearly document the water-particle
289 contact time as an important driver of adsorption of elements and metals in aquatic systems of streams
290 and rivers (Worman, 1998; Worman et al., 1998; Hindshaw et al., 2019; Liu-Lu et al., 2022). Thus, we
291 posit that particulate ε_{Nd} would be sensitive to riverine discharge (Q) if the ε_{Nd} values of the dissolved
292 and SPM phases are different. A higher degree of Nd adsorption during the low flow period (LQ),
293 relative to the high flow period (HQ), would result in positive values of $\Delta\varepsilon_{Nd}^{LQ\text{-}HQ}$ in the SPM if the waters
294 have a higher ε_{Nd} value than the SPM. On the contrary, negative values of $\Delta\varepsilon_{Nd}^{LQ-HQ}$ would result from the
295 SPM having more radiogenic Nd than the waters. In case of insignificant ε_{Nd} difference between the river
296 water and SPM, the $\Delta\varepsilon_{Nd}^{LQ\text{-}HQ}$ values would be indistinguishable from zero.

297 **3.3. Discharge dependency of river particulate ε_{Nd}**

298 We re-evaluated available discharge and particulate ε_{Nd} data of fourteen rivers covering a
299 latitudinal extent of 40˚ S to 40˚ N. They are Uruguay, Parana and Changjiang in the low- to mid-
300 latitudes, Ganga, Brahmaputra and Minjiang in the low latitudes, and Amazon, Orinoco, Maroni,
301 Solimoes, Madeira, Tumbes, Xingu and Tapajos in the tropics. The river lengths range from 230 km
302 (Tumbes River) to 6400 km (Amazon River) and the basin areas vary from 5×10^3 km^2 (Tumbes River)
303 to 6×10^6 km^2 (Amazon River). The annual discharges of these rivers vary over four orders of magnitude,
304 from 4 km^3 to 6300 km^3. Together these rivers contribute ~43% of the global river water flux (Palmer
305 and Edmond, 1993; Henry et al., 1996; Dai et al., 2002; Viers et al., 2008; Do et al., 2020; Jian et al.,

306 2020b; Moquet et al., 2020). The drainage basins are characterized by basaltic (Uruguay), sedimentary
307 (Parana), and mixed lithologies (the rest).

308 To elucidate the impact of solid-solution interaction time, nine sets of time-series particulate ε_{Nd}
309 data of eight rivers were first evaluated (Supplementary Table ST4). This approach is based on the
310 knowledge that water discharge influences the residence time of water in river catchments over seasonal
311 and annual timescales (Manaka et al., 2017; Hindshaw et al., 2019; Liu-Lu et al., 2022; Zhang et al.,
312 2022). Therefore, timeseries data of riverine particulate ε_{Nd} can provide insight into duration of solid-
313 solution interaction and its impact on particulate ε_{Nd}. In addition, catchment scale time-series data limits
314 the impact of variable source rock composition and topography of a river basin, at least for smaller
315 catchments. We argue that if the ε_{Nd} of river water is higher than their conjugate SPM, then the ε_{Nd} of the
316 SPM will have a discharge dependent signature, with low-discharge periods characterised by higher
317 particulate ε_{Nd}. Therefore, for our hypothesis to be valid, an inverse relationship between Q and
318 particulate ε_{Nd} should be observed in each individual river catchment.

319 There are indeed significant ε_{Nd}–Q inverse relationships observed individually for each of the
320 eight in nine sets of time-series particulate ε_{Nd} data (Supplementary Table ST5, Fig. 5). In addition, out
321 of discrete seasonal data available for eight rivers, inverse ε_{Nd}–Q variation trends are observed for each
322 of the six rivers (see Supplementary Note SN5 for more details on river data). A global ε_{Nd}–Q inverse
323 relationshiop for the combined time-series data of all the rivers is neither observed nor anticipated given
324 that the SPM are derived from lithologies that are characterized by distinctly different ε_{Nd} values. Our
325 hypothesis dictates that the ε_{Nd} values of sediments, once generated via weathering of the source rocks in
326 a river catchment, would be modulated during transport by responding to variable water discharge as

explained above. To calculate the mean particulate ε_{Nd} of a flow regime, the time-series data were appropriately averaged after excluding the outliers resulting from unusual fluctuations (see Supplementary Note SN6, Supplementary Table ST4). As predicted, the mean ε_{Nd} values during lean flow periods are higher than high flow periods, with $\Delta\varepsilon_{Nd}^{LQ\text{-}HQ}$ varying in the range of 0.30 to 2.94 units. Similarly, the discrete seasonal data for six rivers demonstrate that the particulate ε_{Nd} values are more radiogenic, by up to 2.52 units, during low flow periods compared to high flow conditions (Supplementary Table ST4). Therefore, observations based on both time-series and discrete seasonal data reinforce our hypothesis that the particulate ε_{Nd} values are modulated by Nd adsorption during riverine transport. In addition, the ε_{Nd}–Q relationship of the rivers provides support to the idea that rivers waters have higher ε_{Nd} than their conjugate SPM, consistent with existing studies on rivers (Henry et al., 1996; Aubert et al., 2001; Rickli et al., 2013; Chatterjee and Singh, 2014; Merschel et al., 2017; Hindshaw et al., 2018).

3.4. Importance of water-particle interaction time

The global particulate ε_{Nd}–Q relationship (Fig. 5), is consistent with laboratory studies (Harvey et al., 1996; Worman, 1998), field investigations (Worman et al., 1998; Manaka et al., 2017; Hindshaw et al., 2019; Liu-Lu et al., 2022; Zhang et al., 2022) and modelling (Worman, 1998; Worman et al., 1998) that document the fluid-particle interaction time as a dominant parameter in the adsorption of dissolved elements in freshwater systems. Studies based on natural and synthetic adsorbent materials report the metal adsorption kinetics to be fast, ranging from a few minutes to a few days (Davranche et al., 2005; Ashour et al., 2017; Mosai et al., 2019; Briao et al., 2021) for reaching equilibrium concentrations in the solid phase. Unfortunately, studies on timescale of metal transport in natural environment of streams and

348 rivers are rather sparse. Limited bodies of work, based on a ^{51}Cr tracer, indicate that the transport
349 timescales of metals are much longer than what the laboratory experiments suggest (Worman, 1998;
350 Worman et al., 1998; Johansson et al., 2001). Notably, these studies show that the removal timescales of
351 reactive metals in natural waters vary as a function of water-particle interaction time and the length of
352 transport.

353 The ε_{Nd}–Q relationship holds good for a set of global rivers (Fig. 5) characterised by discharges
354 that vary by five orders of magnitude and river lengths as high as a few thousand kilometres. Such an
355 observation implies that adsorption reactions take longer time to reach equilibrium in rivers than in the
356 laboratory experiments, consistent with inferences drawn from studies on metal transport in rivers
357 (Worman, 1998; Worman et al., 1998; Johansson et al., 2001). The slower kinetics of Nd adsorption in
358 rivers, as implied from ε_{Nd}–Q relationship (Fig. 5), could be a result of one or a combination of the
359 following reasons: (i) the stability of rare earth complexes with carbonate ions and organic ligands is pH
360 dependent and therefore, the adsorption of REE would be limited particularly at elevated pH (Goldstein
361 and Jacobsen, 1987; Adebayo et al., 2018), (ii) the mass of adsorbent materials such as Fe-Mn
362 oxyhydroxides per unit volume of water (dose rate) are significantly lower in the rivers than those used
363 in laboratory studies, (iii) the stability of Fe-Mn oxyhydroxides may respond to local changes in redox
364 state via processes such as organic matter metabolization (Aucour et al., 2003; Neidhardt et al., 2014)
365 which would adversely impact Nd adsorption if the adsorbent material(s) become thermodynamically
366 unstable during transport. (iv) the presence of materials such as quartz in the river SPM reduces the
367 adsorption potential of SPM. Available studies indicate that cases of slow adsorption kinetics are better
368 explained by the nature of adsorbent materials rather than simple kinetic mechanisms (Ashour et al.,
369 2017; Mosai et al., 2019).

The indisputable support for the idea that the difference of water-particle interaction times between the flow regimes exerts a dominant influence on the particulate ε_{Nd} via adsorption of dissolved Nd comes from the observation that the differences of ε_{Nd} values between the lean and peak flow periods ($\Delta\varepsilon_{Nd}^{LQ\text{-}HQ}$) scale with the magnitude of discharge contrast (Q_c) between these periods (Fig. 6). Furthermore, the discrete seasonal data (Fig. 6) for six rivers e also support the above inference drawn based on the time-series data and therefore support our interpretative framework. However, we advocate caution about the pitfalls associated with unusual fluctuations in the discrete seasonal data that may bias the estimates of ε_{Nd}^{LQ} and ε_{Nd}^{HQ} values. Mass dependent Nd isotope fractionation, although reported for Nd adsorption onto oxyhydroxide phases such as goethite, does not bias the radiogenic isotope composition, i.e. the ε_{Nd} values (Bai et al., 2023). It is intuitive to reason that the $\Delta\varepsilon_{Nd}^{LQ\text{-}HQ}$ values are unlikely to be impacted as the effect of isotope fractionation, if any, and would be nearly cancelled out while computing the seasonal ε_{Nd} difference. Thus, the effect of mass-dependent fractionation for $\Delta\varepsilon_{Nd}^{LQ\text{-}HQ}$ is excluded in subsequent discussions.

The signature of seasonal variation of adsorption of dissolved Nd would be best captured in the particulate ε_{Nd} rather than in the [Nd] or Nd/Al ratios because one or a combination of the following reasons: (i) the Nd concentrations are measured with a precision of a few percent at best. Therefore, adsorption accounting for up to a few percent Nd in the SPM may not be clearly discernible, whereas the associated changes in ε_{Nd} is easily detected due to the higher precision of isotopic measurements; (ii) given that adsorption of Nd is influenced by the abundance of secondary phases such as clay minerals and Fe-Mn oxyhydroxides, the change in concentrations of Nd will be in the same direction as that of Al, Fe or Mn. Therefore, the change in the ratios (Nd/Al, Fe/Al or Mn/Al) in response to Nd adsorption

would be harder to distinguish between periods of low and high flow conditions; (iii) the modulation of particulate ε_{Nd} via adsorption of dissolved Nd would be a function of ε_{Nd} differences between the river water and the SPM ($\Delta\varepsilon_{Nd}^{Riv\text{-}SPM}$), in addition to the degree of Nd adsorption. Therefore, the change in particulate ε_{Nd} would be higher and easily detectable even for a small quantity of Nd adsorbed, provided the $\Delta\varepsilon_{Nd}^{Riv\text{-}SPM}$ is considerable. Lack of combined data on [Nd] and ε_{Nd} in the river water, SPM and adsorbed phases does not allow us to quantitatively evaluate the quantitative impact of ($\Delta\varepsilon_{Nd}^{Riv-SPM}$) vis-à-vis degree of Nd adsorption on the particulate ε_{Nd}. Nevertheless, we demonstrate the coupled impact of these two driving parameters on the particulate $\Delta\varepsilon_{Nd}$ (see Supplementary Note SN7) through a simple mass-balance model. For example, a $\Delta\varepsilon_{Nd}^{LQ\text{-}HQ}$ value of 1 can be achieved at ~6-10% difference of Nd adsorption between the flow regimes (Δf_{Nd}^{LQ-HQ}) if $\Delta\varepsilon_{Nd}^{Riv-SPM}$ values are in the range of 10-15. However, it would require a value of ~20% Δf_{Nd}^{LQ-HQ} to meet the same $\Delta\varepsilon_{Nd}^{LQ\text{-}HQ}$ if $\Delta\varepsilon_{Nd}^{Riv-SPM}$ is decreased to 5 (Supplementary Fig. SF4).

The degree of Nd adsorption and its impact on particulate ε_{Nd} would depend on, in addition to solid-solution contact time, a number of other factors such as: solution pH, abundance and stability of adsorbents such as Fe-Mn oxyhydroxides, the $\Delta\varepsilon_{Nd}$ between SPM and water, and the initial [Nd] of SPM before initiation of adsorption. Despite such complexities, our evaluation and interpretative framework of riverine transport driven modulation of particulate ε_{Nd} is supported by the data of rivers that account for ~43 % of the global water flux and cover wide lithological, geographical and climate variation. Therefore, existing data support the proposition that the transport timescale exerts a dominant control on the riverine particulate ε_{Nd} values on a global scale.

3.5. Role of SPM load and its characteristics

412 A closer inspection of the discharge and SPM data reveals that the water residence times in the
413 catchments exert an indirect control on Nd adsorption by impacting the quantity and the nature (physical
414 and chemical properties) of the SPM. Compared to the low flow periods, the peak flow periods usually
415 have higher SPM concentrations and lower CIA values (Supplementary Fig. SF5). In addition, with the
416 exception of the Changjiang River data, particulate Fe/Al and Mn/Al ratios show inverse correlations
417 with the SPM concentrations (Supplementary Fig. SF6). These observations together indicate that
418 formation of secondary phases, particularly the Fe-Mn oxyhydroxides, is favoured more during the dry
419 periods due to higher water residence time (Ingri and Widerland, 1994; Land et al., 1999; Smith and Liu,
420 2018). As a consequence, Nd adsorption is favourably impacted in the lean periods due to both longer
421 water-particle contact time and higher proportions of adsorbent phases. This idea draws further support
422 from available time-series data in terms of inverse correlations of Nd/Al ratios with the SPM
423 concentrations (Supplementary Fig. SF7), Mn/Al, and Fe/Al ratios barring the Madeira River data
424 (Supplementary Fig. SF8). The weak to moderately strong correlations shown in supplementary figures
425 SF5 – SF8 should not be viewed to undermine our interpretation that the physical and chemical
426 characteristics of the SPM influence Nd adsorption. This is because the distributions of Nd in the river
427 water and the SPM are also regulated by organic complexes, the importance of which has not assessed in
428 this study.

429 **3.6. Impact of length and duration of river transport on particulate ε_{Nd}**

430 The cumulative water-particle contact time in rivers is a function of both the residence time of
431 water (regulated by water discharge) as well as length over which the transport takes place. Available
432 studies document importance of both these factors in regulating the solid-solution interaction processes
433 during stream transport (Worman, 1998; Johansson et al., 2001; Hindshaw et al., 2019; Liu et al., 2019;

Liu-Lu et al., 2022). The influence of transport length on particulate ε_{Nd} is clearly evident in the plot of $\Delta\varepsilon_{Nd}^{LQ\text{-}HQ}$ vs. the length of the rivers (Fig. 7). A strong negative correlation is supportive of the idea that as the degree of Nd adsorption increases and approaches closer to equilibrium due to longer transport, the $\Delta\varepsilon_{Nd}^{LQ\text{-}HQ}$ decreases. Therefore, the relationships of $\Delta\varepsilon_{Nd}^{LQ\text{-}HQ}$ with discharge contrast (Fig. 6) and river length (Fig. 7) demonstrate the combined influence of both the length and duration of riverine transport on the seasonal difference of the particulate ε_{Nd}. If differential inputs from lithologies and their mixing were important, the $\Delta\varepsilon_{Nd}^{LQ\text{-}HQ}$ values would have been higher for large rivers owing to more diverse lithologies expected in larger basins. However, the observed inverse correlation (Fig. 7), in contrast, lends credence to our contention that the impact of variable inputs from lithologies on seasonal particulate ε_{Nd} data is far less significant compared to the duration and length of riverine transport.

3.7. Evaluation of alternative mechanisms

The observed particulate ε_{Nd}–Q relationship (Fig. 5) needs to be evaluated for alternative causative mechanisms. Firstly, the flow regimes may cause preferential erosion and weathering of specific lithology due to differential flow paths (Ibarra et al., 2016; Zhong et al., 2017). Therefore, discharge variation can result in variable particulate ε_{Nd} due to differential lithological inputs between flow regimes, at least in catchments with mixed lithologies. Additionally, river transport can cause hydrodynamic size sorting of particulate matter and different size fractions can be sourced from different lithologies (Bouchez et al., 2011; Garcon and Chauvel, 2014; Bayon et al., 2020a). For example, basaltic particles have been suggested to be preferentially transported with the finer size fractions in the riverine SPM (Garcon and Chauvel, 2014; Bayon et al., 2020a). Therefore, the observed particulate ε_{Nd}–Q trend can be caused, at least partially, due to variable mixing of SPM derived from different lithologies or

size/mineral fractions. This notion of mixing, however, is not supported as none of the time-series data of rivers considered in this study defines a mixing trend in the ε_{Nd} –$[Nd]^{-1}$ space (Supplementary Fig. SF9). Rousseau et al. 2019, based on trace element composition, invoked mixing of basic and granitic rocks to explain the observed time-series ε_{Nd} variation in the Maroni River SPM. However, the ε_{Nd} –$[Nd]^{-1}$ plot for the Maroni River SPM data does not indicate mixing between two end-members (Supplementary Fig. SF9). While we recognize that time-series data may be partly influenced by mixing of sources in specific catchments, we contend that drastic variation of mixing proportions over seasonal time scales are unlikely to be significant and thus, cannot be the primary cause for the observed ε_{Nd}–Q relationship at a global scale. Secondly, fractionation of REEs is a function of age and differentiated nature of the mantle from which the rocks are derived. Given that the younger rocks produced via mantle melting will be characterized by higher Sm/Nd ratios, the particulate ε_{Nd} can also be influenced by the source rock ages (Goldstein and Jacobsen, 1988; Tricca et al., 1999; Peucker-Ehrenbrink et al., 2010). The effect of source rock age and composition on the particulate ε_{Nd} would be best reflected through an inverse correlation between the depleted mantle model age (T_{DM}) and the $^{147}Sm/^{144}Nd$ ratio (Goldstein and Jacobsen, 1988; Tricca et al., 1999). In contradiction to this expectation, these two parameters define significant positive correlations for each of all the rivers (Fig. 8), thus clearly indicating that the particulate Sm/Nd ratios and ε_{Nd} are more likely controlled by processes of weathering and transport than by the variation in the source rock age and composition. Such an observation further lends credence to our contention that the nature and variability of the source rock compositions play insignificant role in impacting the observed particulate ε_{Nd}–Q variation trends in the time-series and seasonal data, although the source rocks would be important in driving the initial ε_{Nd} value of the sediments generated after weathering in a catchment. More notably, our observations (Fig. 8) caution

against using Nd isotope model ages of the riverine SPM without an appropriate evaluation of the impact of weathering and transport on the Sm/Nd ratio and ε_{Nd} of the riverine particulate matter.

4. Utility of ε_{Nd} difference between leachate and detrital phases as a tracer of glacial-interglacial weathering

Our re-evaluation of published ε_{Nd} data of global rivers indicate that the discharge periods characterized by a large $\Delta\varepsilon_{Nd}^{Riv-SPM}$ or higher Nd adsorption or a combination of both would result in an increased difference in ε_{Nd} between the leachate and residual (detrital) phase of marine sediments ($\Delta\varepsilon_{Nd}^{Leach-Res}$). The temporal variation of $\Delta\varepsilon_{Nd}^{Leach-Res}$ in the glacial-interglacial weathering records from fjords and marine sedimentary archive has been primarily attributed to enhanced incongruent and preferential release of radiogenic Nd during the glacial periods (Jang et al. 2020; Jang et al., 2021; Jang and Nam, 2023). Our study unambiguously demonstrates that both parameters $\Delta\varepsilon_{Nd}^{Riv-SPM}$ and degree of Nd adsorption would modulate the particulate ε_{Nd} and therefore $\Delta\varepsilon_{Nd}^{Leach-Res}$ of marine sediments. Elevated values of $\Delta\varepsilon_{Nd}^{Riv-SPM}$ are expected during glacial periods and during the active phase of tectonism when exposure of fresh rocks is more significant, thus favouring incongruent release of Nd isotopes. Thus, the collective impact of high values of $\Delta\varepsilon_{Nd}^{Riv-SPM}$ and higher degree Nd adsorption due to lower river water discharge (slowdown of the hydrological cycle) would result in higher particulate ε_{Nd} values during the glacial periods. Furthermore, the particle-seawater interaction would result in the release of Nd from the river-borne SPM (Pearce et al., 2013; Jeandel and Oelkers, 2015) having a higher ε_{Nd} during the glacial periods and thereby would elevate the seawater ε_{Nd}. Therefore, the combined effect of adsorption of dissolved Nd in rivers, increased $\Delta\varepsilon_{Nd}^{Riv-SPM}$ and the release of radiogenic Nd from the particulate matter in the oceans would amplify the $\Delta\varepsilon_{Nd}^{Leach-Res}$ values of marine sediments during glacial intervals. Thus, the

results of our study support the application of $\Delta\varepsilon_{Nd}^{Leach-Res}$ of marine sediments as a robust tracer to study the weathering records of glacial-interglacial periods.

5. Conclusions

Our investigation of carefully selected two basaltic weathering profiles and re-evaluation of particulate ε_{Nd} data of global rivers provide the following important results.

- Incongruent behaviour of Nd isotopes is unequivocal as evident from differential release of radiogenic Nd to the fluid phase during chemical weathering of basalts. This behaviour is attributed to preferential weathering of minerals having high Sm/Nd ratios and ε_{Nd} than the parent basalts.
- The ε_{Nd} values of Nd released to the weathering solutions are reliably captured by the oxyhydroxide phases of weathering profiles via adsorption of Nd from the fluid phases.
- These two observations and reports of pervasive adsorption of dissolved Nd in rivers led us to hypothesize that particulate ε_{Nd} would be sensitive to the degree of Nd adsorption in rivers which in turn be influenced by the discharge-regulated duration of particle-water interaction.
- Re-evaluation of discharge and particulate ε_{Nd} data of the time-series and discrete seasonal data of fourteen rivers of the world from different geographical and climate regimes demonstrate the discharge-dependent ε_{Nd} variation, thus supporting the above hypothesis.
- Evaluation of ε_{Nd} differences between high and low discharge periods as a function of seasonal discharge contrast and river lengths indisputably demonstrate that modulation of riverine particulate ε_{Nd} is dominantly influenced by the length and duration of adsorption of dissolved Nd.
- Combined effects of incongruent release of radiogenic Nd, adsorption of dissolved Nd in rivers and riverine SPM-seawater interaction would cause higher ε_{Nd} difference between the leachates and

519 residual detrital phases of marine sediments during the glacial periods. Therefore, our investigation
520 advocates the utilization of $\Delta\varepsilon_{Nd}^{Leach-Res}$ of marine sediments as a robust tracer of studying glacial-
521 interglacial weathering records.

522

523 ## CRediT authorship contribution statement

524 **Anup Kumar Sharma:** Conceptualization, Investigation, Writing - Original Draft, Project
525 administration, Methodology, Validation, Formal analysis. **Tarun Kumar Dalai:** Conceptualization,
526 Investigation, Writing - Original Draft, Writing - Review & Editing, Resources, Supervision, Project
527 administration, Funding acquisition, Methodology, Validation, Formal analysis. **Prem Chand Kisku:**
528 Resources, Data Curation, Validation, Formal analysis. **Jitendra Kumar Pattanaik:** Resources, Data
529 Curation, Validation, Formal analysis. **Sambuddha Misra:** Writing - Review & Editing, Resources,
530 Validation, Data Curation. **Shivansh Verma:** Resources, Validation, Data Curation. **Anil Dutt Shukla:**
531 Resources, Validation, Data Curation.

532 ## Acknowledgements

533 AKS thanks the Indian Council of Scientific and Industrial Research (CSIR), New Delhi for providing
534 research fellowship (Award no.: 09/921(0229)2019-EMR-I). TKD acknowledges the financial support
535 through the ARF grant from IISER Kolkata.

References

Adebayo, S. B., Cui, M., Hong, T., White, C. D., Martin, E. E., Johannesson, K. H., 2018. Rare earth elements geochemistry and Nd isotopes in the Mississippi River and Gulf of Mexico mixing zone. Frontiers in Marine Science 5, 166. https://doi.org/10.3389/fmars.2018.00166

Anderson, S. P., Dietrich, W. E., Torres, R., Montgomery, D. R., Loague, K., 1997. Concentration-discharge relationships in runoff from a steep, unchanneled catchment. Water Resources Research 33, 211-225. https://doi.org/10.1029/96WR02715

Andersson, P. S., Dahlqvist, R., Ingri, J., Gustafsson, O., 2001. The isotopic composition of Nd in a boreal river: a reflection of selective weathering and colloidal transport. Geochimica et Cosmochimica Acta 65, 521-527.https://doi.org/10.1016/S0016-7037(00)00535-4

Ashour, R.M., El-Sayed, R., Abdel-Magied, A.F., Abdel-Khalek, A.A., Ali, M.M., Forsberg, K., Uheida, A., Muhammed, M., Dutta, J., 2017. Selective separation of rare earth ions from aqueous solution using functionalized magnetite nanoparticles: kinetic and thermodynamic studies. Chemical Engineering Journal 327, 286-296. https://doi.org/10.1016/j.cej.2017.06.101

Aubert, D., Stille, P., Probst, A., 2001. REE fractionation during granite weathering and removal by waters and suspended loads: Sr and Nd isotopic evidence. Geochimica et Cosmochimica Acta 65, 387-406. https://doi.org/10.1016/S0016-7037(00)00546-9

Aucour, A. M., Tao, F. X., Moreira-Turcq, P., Seyler, P., Sheppard, S., Benedetti, M. F., 2003. The Amazon River: behaviour of metals (Fe, Al, Mn) and dissolved organic matter in the initial mixing at the Rio Negro/Solimões confluence. Chemical geology 197, 271-285. http://dx.doi.org/10.1016/S0009-2541(02)00398-4

Babechuk, M. G., Widdowson, M., Kamber, B. S., 2014. Quantifying chemical weathering intensity and trace element release from two contrasting basalt profiles, Deccan Traps, India. Chemical Geology 363, 56-75. http://dx.doi.org/10.1016/j.chemgeo.2013.10.027

Babechuk, M. G., Widdowson, M., Murphy, M., Kamber, B. S., 2015. A combined Y/Ho, high field strength element (HFSE) and Nd isotope perspective on basalt weathering, Deccan Traps, India. Chemical Geology 396, 25-41. https://doi.org/10.1016/j.chemgeo.2014.12.017

Bai, Jianghao, Kai Luo, Chao Wu, Zhibing Wang, Le Zhang, Shuang Yan, Songxiong Zhong, Jinlong Ma, Gangjian Wei., 2023. Stable neodymium isotopic fractionation during chemical weathering. Earth and Planetary Science Letters 617, 118260. https://doi.org/10.1016/j.epsl.2023.118260

Banerjee, A., Chakrabarti, R., Mandal, S., 2016. Geochemical anatomy of a spheroidally weathered diabase. *Chemical Geology* 440, 124-138. https://doi.org/10.1016/j.chemgeo.2016.07.008

Baksi, A. K., 2022. Geochemistry and geochronology of the Rajmahal Flood Basalt Province, northeastern India: Genetic links to Kerguelen hotspot activity. Journal of Earth System Science 131, 157. https://doi.org/10.1007/s12040-022-01855-8

572 Bayon, G., Douglas, G. B., Denton, G. J., Monin, L., De Deckker, P., 2020a. Preferential riverine export
573 of fine volcanogenic particles to the southeast Australian margin. Frontiers in Marine Science *7*, 89.
574 https://doi.org/10.3389/fmars.2020.00089

575 Bayon, G., Lambert, T., Vigier, N., De Deckker, P., Freslon, N., Jang, K., Larkin, C. S., Piotrowski, A.
576 M., Tachikawa, K., Thollon, M., Tipper, E. T., 2020b. Rare earth element and neodymium isotope
577 tracing of sedimentary rock weathering. Chemical Geology 553, 119794.
578 https://doi.org/10.1016/j.chemgeo.2020.119794

579 Bayon, G., Toucanne, S., Skonieczny, C., André, L., Bermell, S., Cheron, S., Dennielou, B., Etoubleau,
580 J., Freslon, N., Gauchery, T., Germain, Y., Jorry, S. J., Menot, G., Monin, L., Ponzevera, E., Rouget,
581 M. L., Tachikawa, K., Barrat, J. A., 2015. Rare earth elements and neodymium isotopes in world
582 river sediments revisited. Geochimica et Cosmochimica Acta 170, 17-38.
583 https://doi.org/10.1016/j.gca.2015.08.001

584 Bouchez, J., Gaillardet, J., France-Lanord, C., Maurice, L., Dutra-Maia, P., 2011. Grain size control of
585 river suspended sediment geochemistry: Clues from Amazon River depth profiles. Geochem.
586 Geophys. Geosys. 12. http://dx.doi.org/10.1029/2010GC003380

587 Briao, G. D. V., da Silva, M. G. C., Vieira, M. G. A., 2021. Efficient and selective adsorption of
588 neodymium on expanded vermiculite. Industrial & Engineering Chemistry Research 60, 4962-4974.
589 https://doi.org/10.1021/acs.iecr.0c05979

590 Chatterjee, J., Singh S. K., 2014. Dissolved Nd in the Ganga River system and its flux to the Bay of
591 Bengal, Goldschmidt abstracts. https://goldschmidtabstracts.info/2014/387.pdf

592 Chen, T. Y., Frank, M., Haley, B. A., Gutjahr, M., Spielhagen, R. F., 2012. Variations of North Atlantic
593 inflow to the central Arctic Ocean over the last 14 million years inferred from hafnium and
594 neodymium isotopes. Earth and Planetary Science Letters 353, 82-92.
595 https://doi.org/10.1016/j.epsl.2012.08.012

596 Ciffroy, P., Reyss, J. L., Siclet, F., 2003. Determination of the residence time of suspended particles in
597 the turbidity maximum of the Loire estuary by 7Be analysis. Estuarine, Coastal and Shelf
598 Science 57, 553-568. https://doi.org/10.1016/S0272-7714(02)00339-6

599 Clow, D. W., Mast, M. A., 2010. Mechanisms for chemostatic behavior in catchments: Implications for
600 CO2 consumption by mineral weathering. Chemical Geology 269, 40-51.
601 http://dx.doi.org/10.1016/j.chemgeo.2009.09.014

602 Dai, A., Trenberth, K. E., 2002. Estimates of freshwater discharge from continents: Latitudinal and
603 seasonal variations. Journal of hydrometeorology 3, 660-687. https://doi.org/10.1175/1525-
604 7541(2002)003%3C0660:EOFDFC%3E2.0.CO;2

605 Dang, D. H., Ha, Q. K., Némery, J., Strady, E., 2023. The seasonal variations in the interactions between
606 rare earth elements and organic matter in tropical rivers. Chemical Geology 638, 121711.
607 https://doi.org/10.1016/j.chemgeo.2023.121711

608 Dausmann, V., Gutjahr, M., Frank, M., Kouzmanov, K., Schaltegger, U., 2019. Experimental evidence
609 for mineral-controlled release of radiogenic Nd, Hf and Pb isotopes from granitic rocks during
610 progressive chemical weathering. Chemical Geology 507, 64-84.
611 https://doi.org/10.1016/j.chemgeo.2018.12.024

612 Davranche, M., Pourret, O., Gruau, G., Dia, A., Le Coz-Bouhnik, M., 2005. Adsorption of REE (III)-
613 humate complexes onto MnO2: Experimental evidence for cerium anomaly and lanthanide tetrad
614 effect suppression. Geochimica et Cosmochimica Acta 69, 4825-4835.
615 https://doi.org/10.1016/j.gca.2005.06.005

616 Do, A. T., Sottolichio, A., Huybrechts, N., Gardel, A., 2020. Circulation patterns and implication for fine
617 sediment transport in a preserved tropical estuary: The case of the Maroni (French
618 Guiana). Regional studies in marine science 40, 101493.
619 https://doi.org/10.1016/j.rsma.2020.101493

620 Elderfield, H., Greaves, M. J., 1982. The rare earth elements in seawater. Nature 296, 214-219.
621 https://doi.org/10.1038/296214a0

622 Elderfield, H., Upstill-Goddard, R., Sholkovitz, E. R., 1990. The rare earth elements in rivers, estuaries,
623 and coastal seas and their significance to the composition of ocean waters. Geochimica et
624 Cosmochimica Acta 54, 971-991. https://doi.org/10.1016/0016-7037(90)90432-K

625 Fee, J. A., Gaudette, H. E., Lyons, W. B., Long, D. T., 1992. Rare-earth element distribution in Lake
626 Tyrrell groundwaters, Victoria, Australia. Chemical geology 96, 67-93.
627 https://doi.org/10.1016/0009-2541(92)90122-L

628 Garcon, M., Chauvel, C., 2014. Where is basalt in river sediments, and why does it matter? Earth and
629 Planetary Science Letters 407, 61-69. https://doi.org/10.1016/j.epsl.2014.09.033

630 Garcon, M., Chauvel, C., France-Lanord, C., Limonta, M., Garzanti, E., 2014. Which minerals control
631 the Nd–Hf–Sr–Pb isotopic compositions of river sediments? Chemical Geology 364, 42-55.
632 https://doi.org/10.1016/j.chemgeo.2013.11.018

633 Garzanti, E., Ando, S., France-Lanord, C., Censi, P., Vignola, P., Galy, V., Lupker, M., 2011.
634 Mineralogical and chemical variability of fluvial sediments 2. Suspended-load silt (Ganga–
635 Brahmaputra, Bangladesh). Earth and Planetary Science Letters 302, 107-120.
636 https://doi.org/10.1016/j.epsl.2010.11.043

637 Goldstein, S. J., Jacobsen, S. B., 1987. The Nd and Sr isotopic systematics of river-water dissolved
638 material: Implications for the sources of Nd and Sr in seawater. Chemical Geology: Isotope
639 Geoscience section 66, 245-272. https://doi.org/10.1016/0168-9622(87)90045-5

640 Goldstein, S. J., Jacobsen, S. B., 1988. Nd and Sr isotopic systematics of river water suspended material:
641 implications for crustal evolution. Earth and Planetary Science Letters 87, 249-265.
642 https://doi.org/10.1016/0012-821X(88)90013-1

643 Goldstein, S. L., O'Nions, R. K., Hamilton, P. J., 1984. A Sm-Nd isotopic study of atmospheric dusts
644 and particulates from major river systems. Earth and planetary Science letters 70, 221-236.
645 https://doi.org/10.1016/0012-821X(84)90007-4

646 Gupta S. K., Chen K. Y., 1975. Partitioning of trace metals in selective chemical fractions of near shore
647 sediments. Environmental Letters 10, 129. https://doi.org/10.1080/00139307509435816

648 Harvey, J. W., Wagner, B. J., Bencala, K. E., 1996. Evaluating the reliability of the stream tracer
649 approach to characterize stream-subsurface water exchange. Water resources research 32, 2441-
650 2451. http://dx.doi.org/10.1029/96WR01268

651 Henry, F., Probst, J. L., Thouron, D., Depetris, P., Garçon, V., 1996. Nd-Sr isotopic compositions of
652 dissolved and particulate material transported by the Parana and Uruguay rivers during high
653 (December 1993) and low (September 1994) water periods. Geological Sciences, Bulletins and
654 Memoirs 49, 89-100.

655 Hindshaw, R. S., Aciego, S. M., Piotrowski, A. M., Tipper, E. T., 2018. Decoupling of dissolved and
656 bedrock neodymium isotopes during sedimentary cycling. Geochemical Perspectives Letters 8, 43-
657 46. https://doi.org/10.7185/geochemlet.1828

658 Hindshaw, R. S., Teisserenc, R., Le Dantec, T., Tananaev, N., 2019. Seasonal change of geochemical
659 sources and processes in the Yenisei River: A Sr, Mg and Li isotope study. Geochimica et
660 Cosmochimica Acta 255, 222-236. https://doi.org/10.1016/j.gca.2019.04.015

661 Horbe, A. M. C., Albuquerque, M. F. D. S., Dantas, E. L., 2022. Nd and Sr Isotopes and REE
662 Investigation in Tropical Weathering Profiles of Amazon Region. Frontiers in Earth Science 10,
663 845224. https://doi.org/10.3389/feart.2022.845224

664 Ibarra, D. E., Caves, J. K., Moon, S., Thomas, D. L., Hartmann, J., Chamberlain, C. P., Maher, K., 2016.
665 Differential weathering of basaltic and granitic catchments from concentration–discharge
666 relationships. Geochimica et Cosmochimica Acta 190, 265-293.
667 https://doi.org/10.1016/j.gca.2016.07.006

668 Ingri, J., Widerlund, A., 1994. Uptake of alkali and alkaline-earth elements on suspended iron and
669 manganese in the Kalix River, northern Sweden. Geochimica et Cosmochimica Acta 58, 5433-5442.
670 https://doi.org/10.1016/0016-7037(94)90240-2

671 Ingri, J., Widerlund, A., Land, M., Gustafsson, Ö., Andersson, P., Ohlander, B. (2000) Temporal
672 variations in the fractionation of the rare earth elements in a boreal river; the role of colloidal
673 particles. Chemical Geology 166, 23-45. https://doi.org/10.1016/S0009-2541(99)00178-3

674 Jang, K., Ahn, Y., Joe, Y.J., Braun, C.A., Joo, Y.J., Kim, J.H., Bayon, G., Forwick, M., Vogt, C., Nam,
675 S.I., 2021. Glacial and environmental changes in northern Svalbard over the last 16.3 ka inferred
676 from neodymium isotopes. Global and Planetary Change 201, 103483.
677 https://doi.org/10.1016/j.gloplacha.2021.103483

678 Jang, K., Bayon, G., Han, Y., Joo, Y. J., Kim, J. H., Ryu, J. S., Woo, J., Forwick, M., Szczuciński, W.,
679 Kim, J. H., Nam, S. I., 2020. Neodymium isotope constraints on chemical weathering and past

glacial activity in Svalbard. Earth and Planetary Science Letters 542, 116319. https://doi.org/10.1016/j.epsl.2020.116319

Jang, K., Bayon, G., Han, Y., Joo, Y. J., Kim, J. H., Ryu, J. S., Woo, J., Forwick, M., Szczuciński, W., Kim, J. H., Nam, S. I., 2020b. Neodymium isotope constraints on chemical weathering and past glacial activity in Svalbard. Earth and Planetary Science Letters 542, 116319. https://doi.org/10.1016/j.epsl.2020.116319

Jang, K., Nam, S. I., 2023 Application of Sedimentary Neodymium Isotopes to the Reconstruction of the Arctic Paleoceanography. Ocean and Polar Research 45, 89-102. https://doi.org/10.4217/OPR.2023005

Jeandel, C., Oelkers, E. H., 2015. The influence of terrigenous particulate material dissolution on ocean chemistry and global element cycles. Chemical Geology 395, 50-66. https://doi.org/10.1016/j.chemgeo.2014.12.001

Jian, X., Yang, S., Hong, D., Liang, H., Zhang, S., Fu, H., Zhang, W., 2020a. Seasonal geochemical heterogeneity of sediments from a subtropical mountainous river in SE China. Marine Geology 422, 106120. https://doi.org/10.1016/j.margeo.2020.106120

Jian, X., Zhang, W., Yang, S., Kao, S. J., 2020b. Climate-dependent sediment composition and transport of mountainous rivers in tectonically stable, subtropical East Asia. Geophysical Research Letters 47, e2019GL086150. https://doi.org/10.1029/2019GL086150

Johansson, H., Jonsson, K., Forsman, K. J., Worman, A., 2001. Retention of conservative and sorptive solutes in streams—simultaneous tracer experiments. Science of the total environment 266, 229-238. https://doi.org/10.1016/S0048-9697(00)00758-0

Kisku, P. C., Kumar, H., Pattanaik, J. K., 2020. Hydrogeochemical Study of Morang River Draining Rajmahal Basalt: Implication to Mineral Equilibria and Chemical Weathering. Proceedings of the Indian National Science Academy 86, 1239-1257. http://dx.doi.org/10.16943/ptinsa/2020/155493

Land, M., Ohlander, B., Ingri, J., Thunberg, J., 1999. Solid speciation and fractionation of rare earth elements in a spodosol profile from northern Sweden as revealed by sequential extraction. Chemical Geology 160, 121-138. https://doi.org/10.1016/S0009-2541(99)00064-9

Larkin, C.S., Piotrowski, A.M., Hindshaw, R.S., Bayon, G., Hilton, R.G., Baronas, J.J., Dellinger, M., Wang, R., Tipper, E.T., 2021. Constraints on the source of reactive phases in sediment from a major Arctic River using neodymium isotopes. Earth and Planetary Science Letters 565, p.116933.https://doi.org/10.1016/j.epsl.2021.116933

Lei, H. L., Yang, T., Jiang, S. Y., Pu, W., 2019. A simple two-stage column chromatographic separation scheme for strontium, lead, neodymium and hafnium isotope analyses in geological samples by thermal ionization mass spectrometry or multi-collector inductively coupled plasma mass spectrometry. Journal of Separation Science 42, 3261-3275. https://doi.org/10.1002/jssc.201900579

Leybourne, M. I., Cousens, B. L., 2005. Rare earth elements (REE) and Nd and Sr isotopes in groundwater and suspended sediments from the Bathurst Mining Camp, New Brunswick: water-

717 rock reactions and elemental fractionation. Rare Earth Elements in Groundwater Flow Systems,
718 253-293. https://doi.org/10.1007/1-4020-3234-X_10

719 Liu, H., Guo, H., Pourret, O., Chen, Y., Yuan, R., 2019. Role of manganese oxyhydroxides in the
720 transport of rare earth elements along a groundwater flow path. International journal of
721 environmental research and public health 16, 2263. https://doi.org/10.3390/ijerph16132263

722 Liu, X. M., Rudnick, R. L., McDonough, W. F., Cummings, M. L., 2013. Influence of chemical
723 weathering on the composition of the continental crust: Insights from Li and Nd isotopes in bauxite
724 profiles developed on Columbia River Basalts. Geochimica et Cosmochimica Acta 115, 73-91.
725 http://dx.doi.org/10.1016/j.gca.2013.03.043

726 Liu-Lu, B., Jin, Z., Gou, L. F., Zhang, F., He, M. Y., Xu, Y., 2022. Seasonal River chemistry and lithium
727 isotopes in the Min Jiang at eastern Tibetan Plateau: roles of silicate weathering and hydrology.
728 Frontiers in Earth Science 10, 838867. https://doi.org/10.3389/feart.2022.838867

729 Ma, J. L., Wei, G. J., Xu, Y. G., Long, W. G., Sun, W. D., 2007. Mobilization and re-distribution of major
730 and trace elements during extreme weathering of basalt in Hainan Island, South China. Geochimica
731 et Cosmochimica Acta 71, 3223-3237. https://doi.org/10.1016/j.gca.2007.03.035

732 Ma, J., Wei, G., Xu, Y., Long, W., 2010. Variations of Sr–Nd–Hf isotopic systematics in basalt during
733 intensive weathering. Chemical Geology 269, 376-385.
734 https://doi.org/10.1016/j.chemgeo.2009.10.012

735 Manaka, T., Araoka, D., Yoshimura, T., Hossain, H. Z., Nishio, Y., Suzuki, A., Kawahata, H., 2017.
736 Downstream and seasonal changes of lithium isotope ratios in the Ganges-Brahmaputra River
737 system. Geochemistry, Geophysics, Geosystems 18, 3003-3015.
738 https://ui.adsabs.harvard.edu/link_gateway/2017GGG....18.3003M/doi:10.1002/2016GC006738

739 Martin, C. E., McCulloch, M. T., 1999. Nd-Sr isotopic and trace element geochemistry of river
740 sediments and soils in a fertilized catchment, New South Wales, Australia. Geochimica et
741 Cosmochimica Acta 63, 287-305. https://doi.org/10.1016/S0016-7037(98)00308-1

742 McGuire, K. J., McDonnell, J. J., 2006. A review and evaluation of catchment transit time
743 modeling. Journal of Hydrology 330, 543-563. https://doi.org/10.1016/j.jhydrol.2006.04.020

744 Merschel, G., Bau, M., Schmidt, K., Münker, C., Dantas, E. L., 2017. Hafnium and neodymium isotopes
745 and REY distribution in the truly dissolved, nanoparticulate/colloidal and suspended loads of rivers
746 in the Amazon Basin, Brazil. Geochimica et Cosmochimica Acta 213, 383-399.
747 https://doi.org/10.1016/j.gca.2017.07.006

748 Moquet, J.S., Morera, S., Turcq, B., Poitrasson, F., Roddaz, M., Moreira-Turcq, P., Espinoza, J.C.,
749 Guyot, J.L., Takahashi, K., Orrillo-Vigo, J., Petrick, S., Mounic, S., Sondag, F., 2020. Control of
750 seasonal and inter-annual rainfall distribution on the Strontium-Neodymium isotopic compositions
751 of suspended particulate matter and implications for tracing ENSO events in the Pacific coast
752 (Tumbes basin, Peru). Global and Planetary Change 185, 103080.
753 https://doi.org/10.1016/j.gloplacha.2019.103080

754 Mosai, A. K., Chimuka, L., Cukrowska, E. M., Kotzé, I. A., Tutu, H., 2019. The recovery of rare earth
755 elements (REEs) from aqueous solutions using natural zeolite and bentonite. Water, Air, & Soil
756 Pollution 230, 1-17. https://doi.org/10.1007/s11270-019-4236-4

757 Negrel, P., 2006. Water–granite interaction: clues from strontium, neodymium and rare earth elements in
758 soil and waters. Applied Geochemistry 21, 1432-1454.
759 https://doi.org/10.1016/j.apgeochem.2006.04.007

760 Negrel, P., Casanova, J., Blomqvist, R., 2001. Nd isotopes and water mixing phenomena in
761 groundwaters from Palmottu (Finland). Water research, 35, 1617-1623.
762 https://doi.org/10.1016/S0043-1354(00)00569-8

763 Neidhardt, H., Berner, Z.A., Freikowski, D., Biswas, A., Majumder, S., Winter, J., Gallert, C.,
764 Chatterjee, D., Norra, S., 2014. Organic carbon induced mobilization of iron and manganese in a
765 West Bengal aquifer and the muted response of groundwater arsenic concentrations. Chemical
766 Geology 367, 51-62. https://doi.org/10.1016/j.chemgeo.2013.12.021

767 Nobre Silva, I. G., Weis, D., Scoates, J. S., 2010. Effects of acid leaching on the Sr-Nd-Hf isotopic
768 compositions of ocean island basalts. Geochem. Geophys. Geosys. 11,
769 https://doi.org/10.1029/2010GC003176

770 Ohlander, B., Ingri, J., Land, M., Schöberg, H., 2000. Change of Sm-Nd isotope composition during
771 weathering of till. Geochimica et Cosmochimica Acta 64, 813-820. https://doi.org/10.1016/S0016-
772 7037(99)00365-8

773 Palmer, M. R., Edmond, J. M., 1993. Uranium in river water. Geochimica et Cosmochimica Acta 57,
774 4947-4955. https://doi.org/10.1016/0016-7037(93)90131-F

775 Pearce, C. R., Jones, M. T., Oelkers, E. H., Pradoux, C., Jeandel, C., 2013. The effect of particulate
776 dissolution on the neodymium (Nd) isotope and Rare Earth Element (REE) composition of
777 seawater. Earth and Planetary Science Letters 369, 138-147.
778 https://doi.org/10.1016/j.epsl.2013.03.023

779 Peucker-Ehrenbrink, B., Miller, M. W., Arsouze, T., Jeandel, C., 2010 Continental bedrock and riverine
780 fluxes of strontium and neodymium isotopes to the oceans. Geochem. Geophys. Geosys. 11.
781 https://doi.org/10.1029/2009GC002869

782 Piepgras, D. J., Wasserburg, G. J., Dasch, E. J., 1979. The isotopic composition of Nd in different ocean
783 masses. Earth and Planetary Science Letters 45, 223-236. https://doi.org/10.1016/0012-
784 821X(79)90125-0

785 Rickli, J., Frank, M., Stichel, T., Georg, R. B., Vance, D., Halliday, A. N., 2013. Controls on the
786 incongruent release of hafnium during weathering of metamorphic and sedimentary
787 catchments. Geochimica et Cosmochimica Acta 101, 263-284.
788 http://dx.doi.org/10.1016/j.gca.2012.10.019

789 Rousseau, T. C., Roddaz, M., Moquet, J. S., Delgado, H. H., Calves, G., Bayon, G., 2019. Controls on
790 the geochemistry of suspended sediments from large tropical South American rivers (Amazon,

Orinoco and Maroni). Chemical Geology 522, 38-54. https://doi.org/10.1016/j.chemgeo.2019.05.027

Shiller, A. M., 2002. Seasonality of dissolved rare earth elements in the lower Mississippi River. Geochemistry, Geophysics, Geosystems 3, 1-14. https://doi.org/10.1029/2002GC000372

Sholkovitz, E. R., 1995. The aquatic chemistry of rare earth elements in rivers and estuaries. Aquatic geochemistry 1, 1-34. https://doi.org/10.1007/BF01025229

Smith, C., Liu, X. M., 2018. Spatial and temporal distribution of rare earth elements in the Neuse River, North Carolina. Chemical Geology 488, 34-43. https://doi.org/10.1016/j.chemgeo.2018.04.003

Spencer, K. J., De Carlo, E. H., McMurtry, G. M., 1996. Isotopic clues to sources of natural and anthropogenic lead in sediments and soils from O'ahu, Hawai'i. Pacific Sci. 49, 492–510. http://hdl.handle.net/10125/2336

Sprenger, M., Stumpp, C., Weiler, M., Aeschbach, W., Allen, S.T., Benettin, P., Dubbert, M., Hartmann, A., Hrachowitz, M., Kirchner, J.W., McDonnell, J.J., 2019. The demographics of water: A review of water ages in the critical zone. Reviews of Geophysics 57, 800-834. https://doi.org/10.1029/2018RG000633

Steinmann, M., Stille, P., 2008. Controls on transport and fractionation of the rare earth elements in stream water of a mixed basaltic–granitic catchment basin (Massif Central, France). Chemical Geology 254, 1-18. https://doi.org/10.1016/j.chemgeo.2008.04.004

Sufke, F., Gutjahr, M., Gilli, A., Anselmetti, F. S., Glur, L., Eisenhauer, A., 2019. Early-stage weathering systematics of Pb and Nd isotopes derived from a high-Alpine Holocene Lake sediment record. Chemical geology 507, 42-53. https://doi.org/10.1016/j.chemgeo.2018.12.026

Tachikawa, K., Roy-Barman, M., Michard, A., Thouron, D., Yeghicheyan, D., Jeandel, C., 2004. Neodymium isotopes in the Mediterranean Sea: Comparison between seawater and sediment signals. Geochimica et Cosmochimica Acta 68, 3095-3106. https://doi.org/10.1016/j.gca.2004.01.024

Tanaka, T., Togashi, S., Kamioka, H., Amakawa, H., Kagami, H., Hamamoto, T., Yuhara, M., Orihashi, Y., Yoneda, S., Shimizu, H., Kunimaru, T., 2000. JNdi-1: a neodymium isotopic reference in consistency with LaJolla neodymium. Chemical Geology 168, 279-281. https://doi.org/10.1016/S0009-2541(00)00198-4

Tipper, E.T., Stevenson, E.I., Alcock, V., Knight, A.C., Baronas, J.J., Hilton, R.G., Bickle, M.J., Larkin, C.S., Feng, L., Relph, K.E., Hughes, G., 2021. Global silicate weathering flux overestimated because of sediment–water cation exchange. Proceedings of the National Academy of Sciences 118, e2016430118. https://doi.org/10.1073/pnas.2016430118

Tricca, A., Stille, P., Steinmann, M., Kiefel, B., Samuel, J., Eikenberg, J., 1999. Rare earth elements and Sr and Nd isotopic compositions of dissolved and suspended loads from small river systems in the Vosges mountains (France), the river Rhine and groundwater. Chemical Geology 160, 139-158. https://doi.org/10.1016/S0009-2541(99)00065-0

Viers, J., Roddaz, M., Filizola, N., Guyot, J.L., Sondag, F., Brunet, P., Zouiten, C., Boucayrand, C., Martin, F., Boaventura, G.R., 2008. Seasonal and provenance controls on Nd–Sr isotopic compositions of Amazon rivers suspended sediments and implications for Nd and Sr fluxes exported to the Atlantic Ocean. Earth and Planetary Science Letters 274, 511-523. https://doi.org/10.1016/j.epsl.2008.08.011

Viers, J., Wasserburg, G. J., 2004. Behavior of Sm and Nd in a lateritic soil profile. Geochimica et Cosmochimica Acta 68, 2043-2054. https://doi.org/10.1016/j.gca.2003.10.034

Wallbrink, P. J., Murray, A. S., Olley, J. M., Olive, L. J., 1998. Determining sources and transit times of suspended sediment in the Murrumbidgee River, New South Wales, Australia, using fallout ^{137}Cs and ^{210}Pb. Water Resources Research 34, 879-887. https://doi.org/10.1029/97WR03471

Wallrich, I. L., Stewart, B. W., Capo, R. C., Hedin, B. C., Phan, T. T., 2020. Neodymium isotopes track sources of rare earth elements in acidic mine waters. Geochimica et Cosmochimica Acta, 269, 465-483. https://doi.org/10.1016/j.gca.2019.10.044

Weis, D., Kieffer, B., Maerschalk, C., Barling, J., De Jong, J., Williams, G. A., Hanano, D., Pretorius, W., Mattielli, N., Scoates, J. S., Goolaerts, A., 2006. High-precision isotopic characterization of USGS reference materials by TIMS and MC-ICP-MS. Geochemistry Geophysics Geosystems 7, 8. https://doi.org/10.1029/2006GC001283

Wilson, D. J., Piotrowski, A. M., Galy, A., Clegg, J. A., 2013. Reactivity of neodymium carriers in deep sea sediments: Implications for boundary exchange and paleoceanography. Geochimica et Cosmochimica Acta 109, 197-221. https://doi.org/10.1016/j.gca.2013.01.042

Worman, A., 1998. Analytical solution and timescale for transport of reacting solutes in rivers and streams. Water Resources Research 34, 2703-2716. https://doi.org/10.1029/98WR01338

Worman, A., Forsman, J., Johansson, H., 1998. Modeling retention of sorbing solutes in streams based on tracer experiment using 51Cr. Journal of environmental engineering 124, 122-130. https://doi.org/10.1061/(ASCE)0733-9372(1998)124:2(122)

Zhang, F., Dellinger, M., Hilton, R. G., Yu, J., Allen, M. B., Densmore, A. L., Jin, Z., 2022. Hydrological control of river and seawater lithium isotopes. Nature Communications 13, 3359. https://doi.org/10.1038/s41467-022-31076-y

Zhong, J., Li, S. L., Tao, F., Ding, H., Liu, J., 2017. Impacts of hydrologic variations on chemical weathering and solute sources in the Min River basin, Himalayan–Tibetan region. Environmental Science and Pollution Research 24, 19126-19137. https://doi.org/10.1007/s11356-017-9584-2

Figures

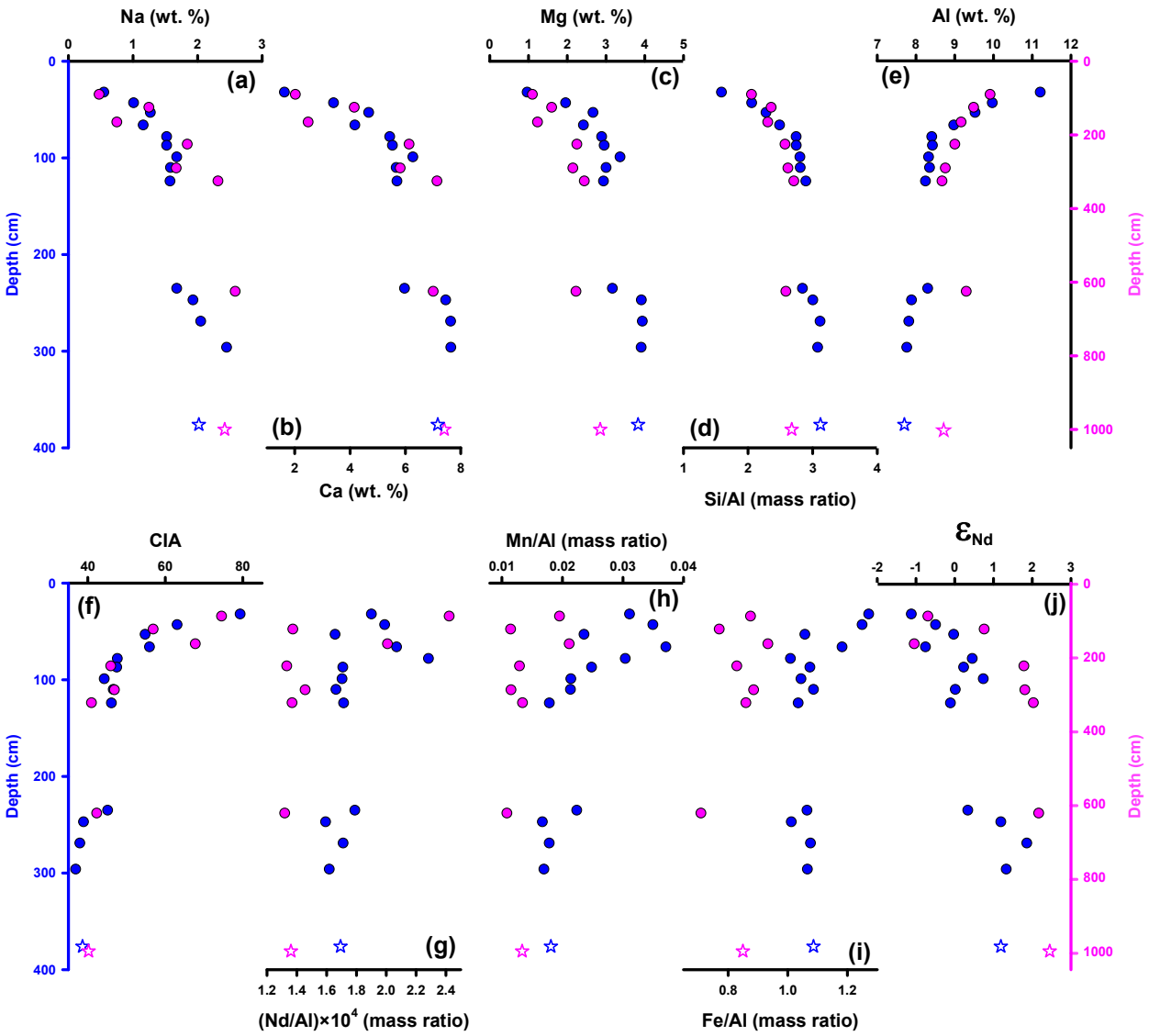

Fig. 1. Signatures of weathering and post-weathering processes (adsorption) with depth in the Dalahi (blue) and Pakuria (pink) weathering profiles. **(a-d):** Chemical weathering drives drop in concentrations of Na, Ca, Mg and Si/Al ratio relative to the parent basalts (stars). **(e):** The concentrations of the immobile element Al, as expected, show increasing upward trends during weathering. **(f):** Progressive chemical weathering is evident from upward increasing values of CIA, consistent with the loss of mobile elements (Na, Ca, Mg and Si). **(g, h, i):** The upward increasing Nd/Al ratios display a general correspondence with Fe/Al and Mn/Al ratios, indicating adsorption of Nd from fluid phase onto oxyhydroxide phases. **(j):** The incongruent behaviour of Nd isotopes during weathering, evident from the upward decreasing trend of ε_{Nd} is most likely driven by differential mineral weathering (see Fig. 2 and text for more details).

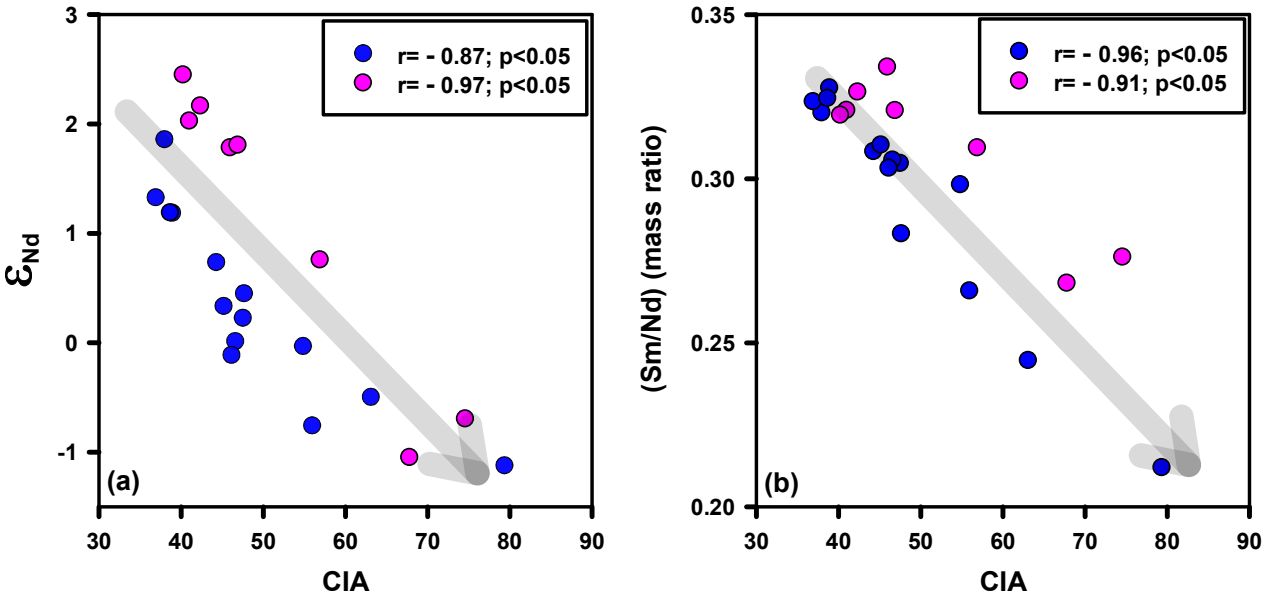

Fig. 2. Incongruent behaviour of Sm, Nd and its isotopes during weathering. The strong inverse correlations of ε_{Nd} **(a)** and Sm/Nd ratio **(b)** with CIA in the Dalahi (blue) and Pakuria (pink) profiles are suggestive of preferential weathering of minerals having higher Sm/Nd ratio and ε_{Nd} compared to the basaltic parent rocks. The directions of increasing degree of chemical weathering are marked with arrows.

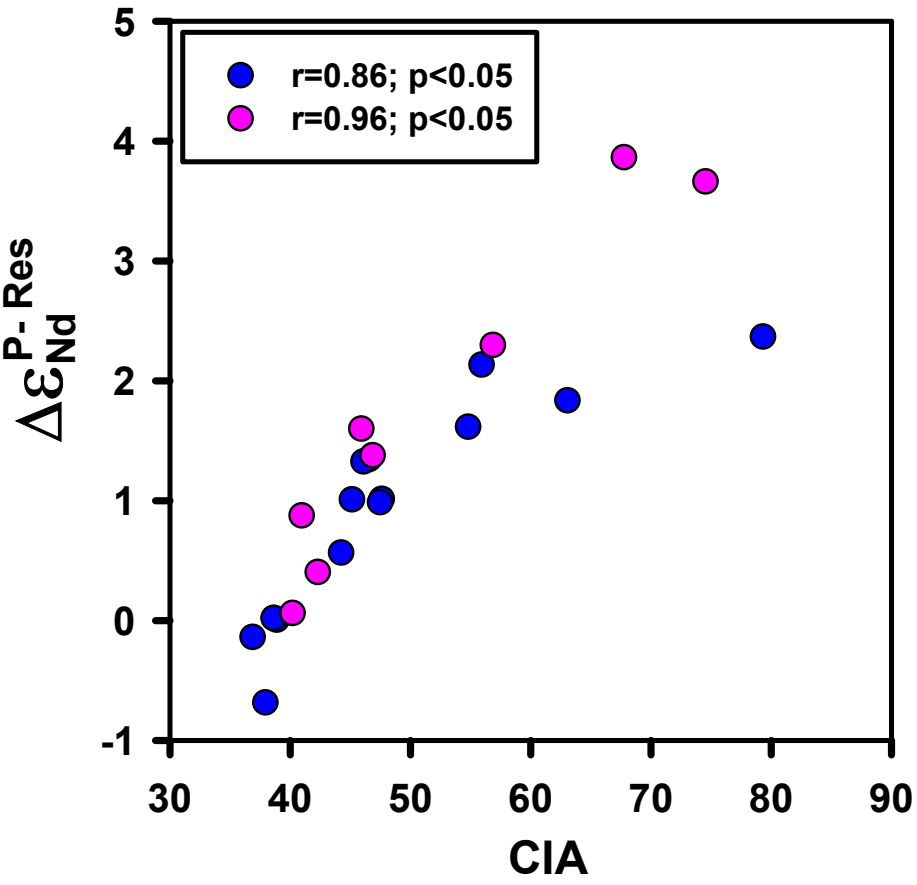

Fig. 3. The incongruent loss of radiogenic Nd to solution during progressive chemical weathering. The ε_{Nd} difference between the parent basalts and the residual phases (Supplementary Note SN4) of the profiles ($\Delta\varepsilon_{Nd}^{P-Res}$) is a measure of ε_{Nd} of the weathering solution. The $\Delta\varepsilon_{Nd}^{P-Res}$ scales with the degree of weathering as evident from its positive correlation with CIA.

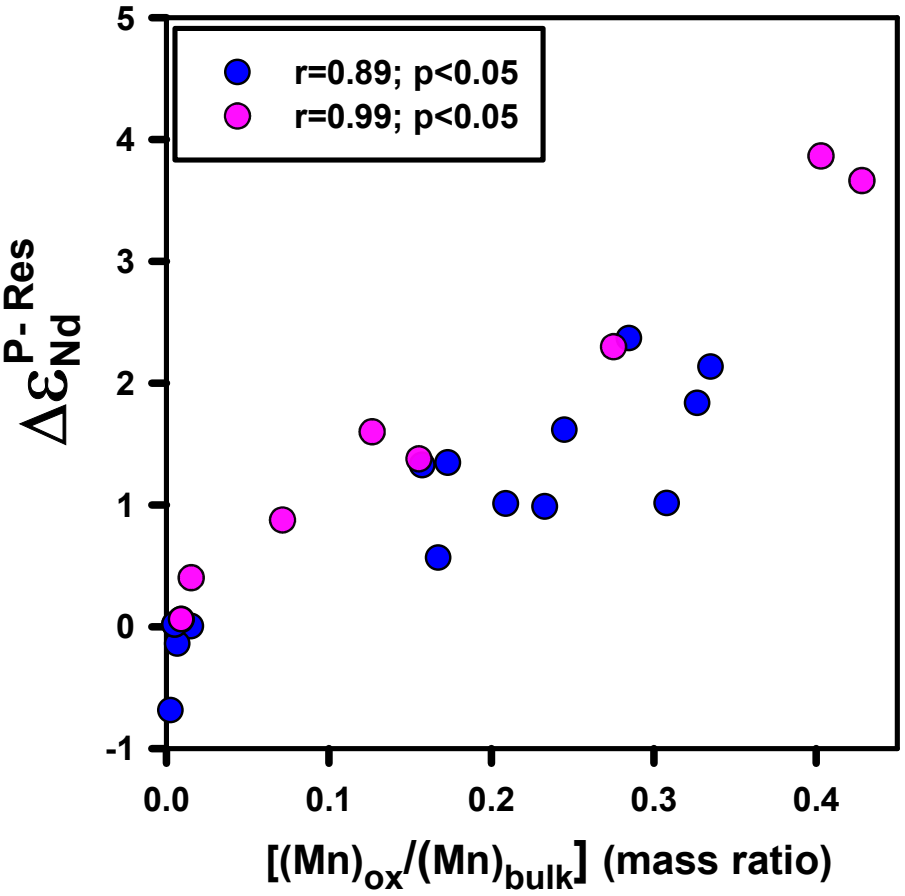

Fig. 4. Oxyhydroxide phases capture ε_{Nd} of Nd released to the weathering solution. The ε_{Nd} of weathering solutions ($\Delta\varepsilon_{Nd}^{P-Res}$) is recorded in Mn oxyhydroxide phases as evident from strong positive correlations observed between $\Delta\varepsilon_{Nd}^{P-Res}$ and ratio of Mn concentrations in the oxyhydroxide to bulk phases ($[Mn]_{ox}/[Mn]_{bulk}$).

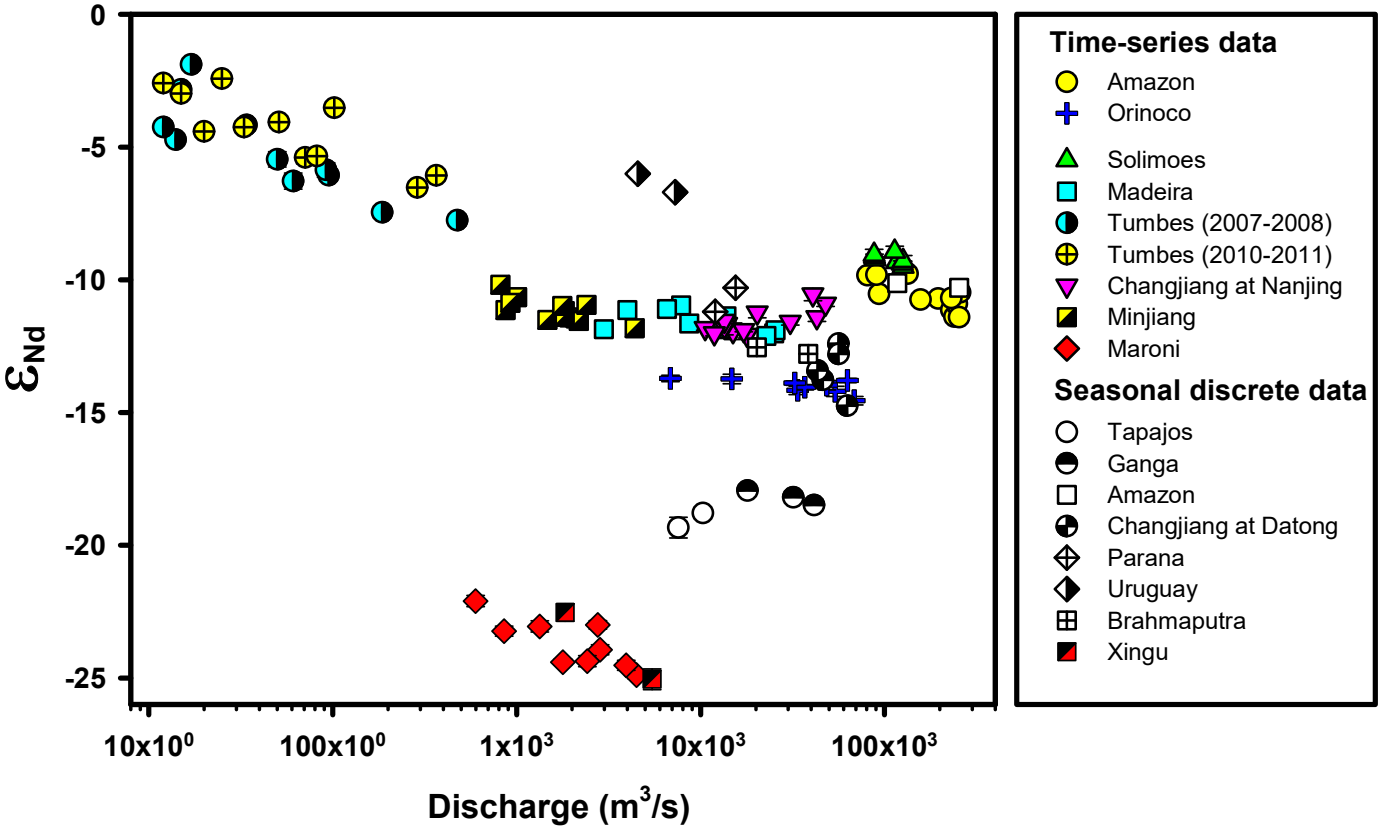

Fig. 5. Dependency of particulate ε_{Nd} of global rivers on the solid-solution interaction time, which is regulated by river water discharge. Both the time-series and discrete seasonal data available in literature are plotted. A general decrease of particulate ε_{Nd} with water discharge is observed individually for each of the river time-series data evaluated in this study. Parameters of regression analysis for the individual river time-series data are listed in supplementary table ST5. Data sources provided in supplementary table ST4. Note that a global inverse correlation for combined data of all the rivers is neither observed nor anticipated (see text for more details).

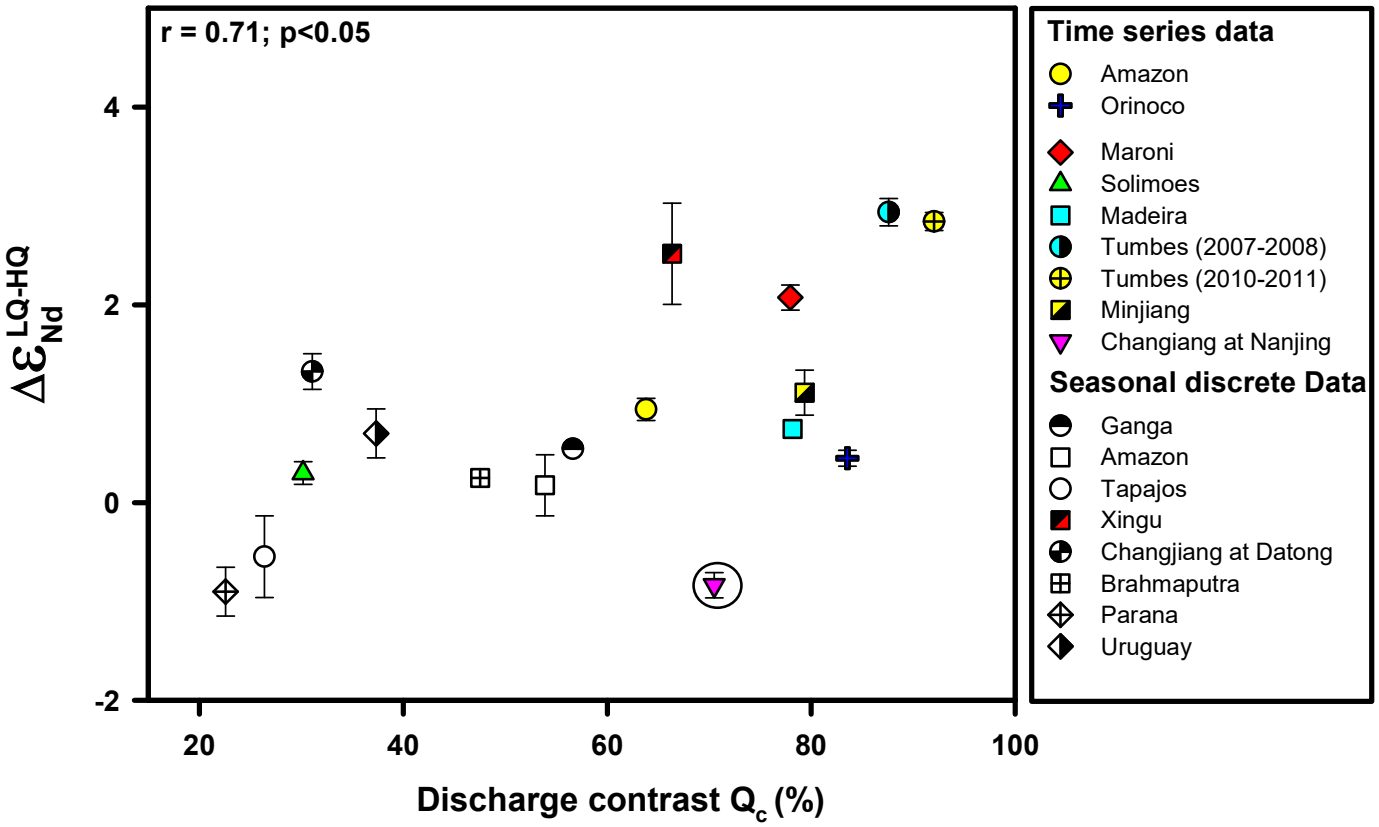

Fig. 6. Impact of seasonal discharge contrast on the difference of particulate ε_{Nd} of rivers between low flow and high flow periods. The difference of mean particulate ε_{Nd} between low discharge (LQ) and high discharge (HQ) periods scales with the magnitude of discharge contrast (Q_c) between the LQ and HQ periods. Such an observation provides irrefutable evidence for the dominating influence of solid-solution interaction time on the modulation of particulate ε_{Nd} of global rivers. Calculations of mean seasonal ε_{Nd} and discharge contrast are detailed in supplementary table ST4 and supplementary note SN6. The outlier (circled) of time-series data of the Changjiang River at Nanjing is excluded from regression (see supplementary note SN5 for more details on this dataset).

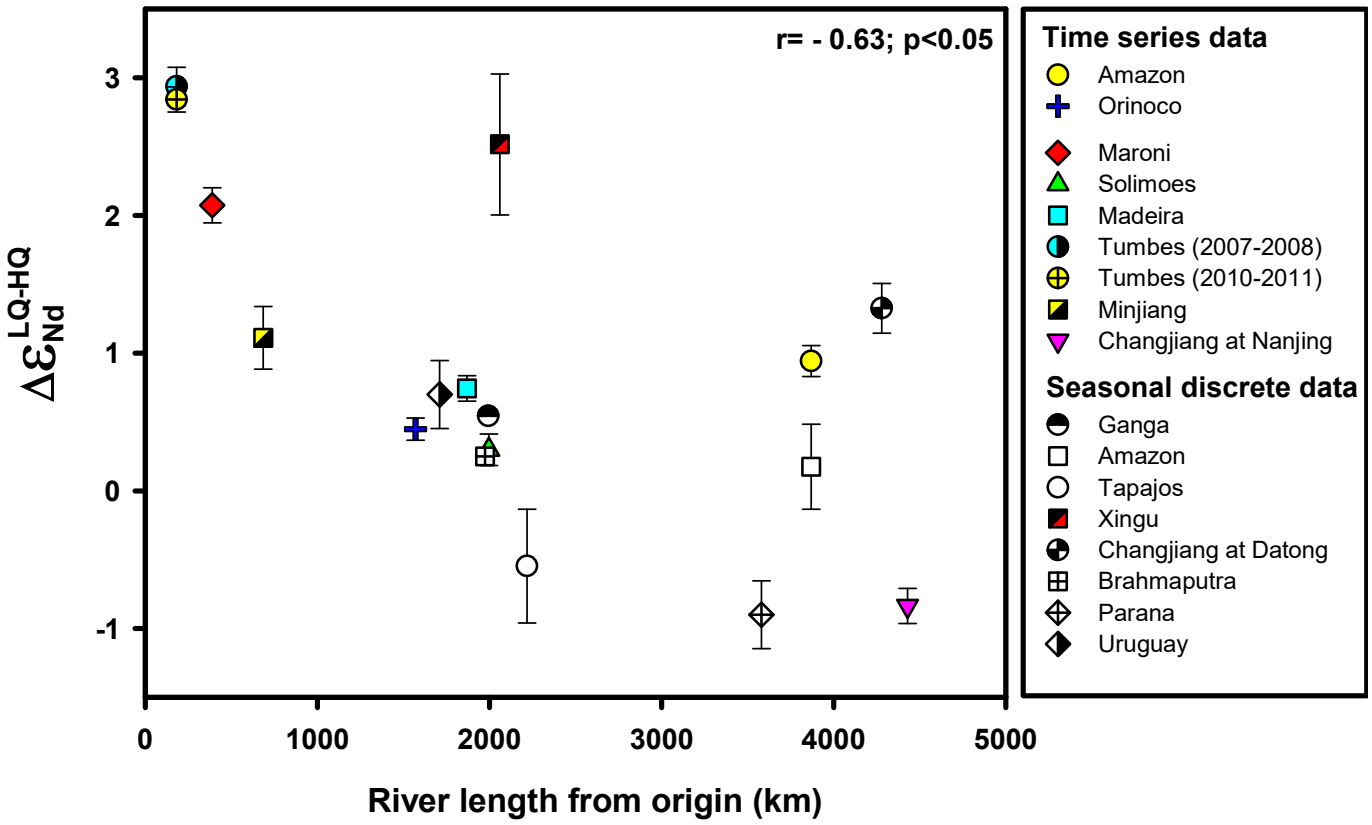

Fig. 7. The influence of transport length on variation of particulate ε_{Nd}. The differences of the particulate ε_{Nd} between the lean (LQ) and peak (HQ) flow periods demonstrate a generally decreasing trend with length of river transport. Such an observation provides the evidence for modulation of particulate ε_{Nd} as a function of length of river transport which influence the adsorption of dissolved Nd via duration of solid-solution interaction. See supplementary table ST4 for the data sources.

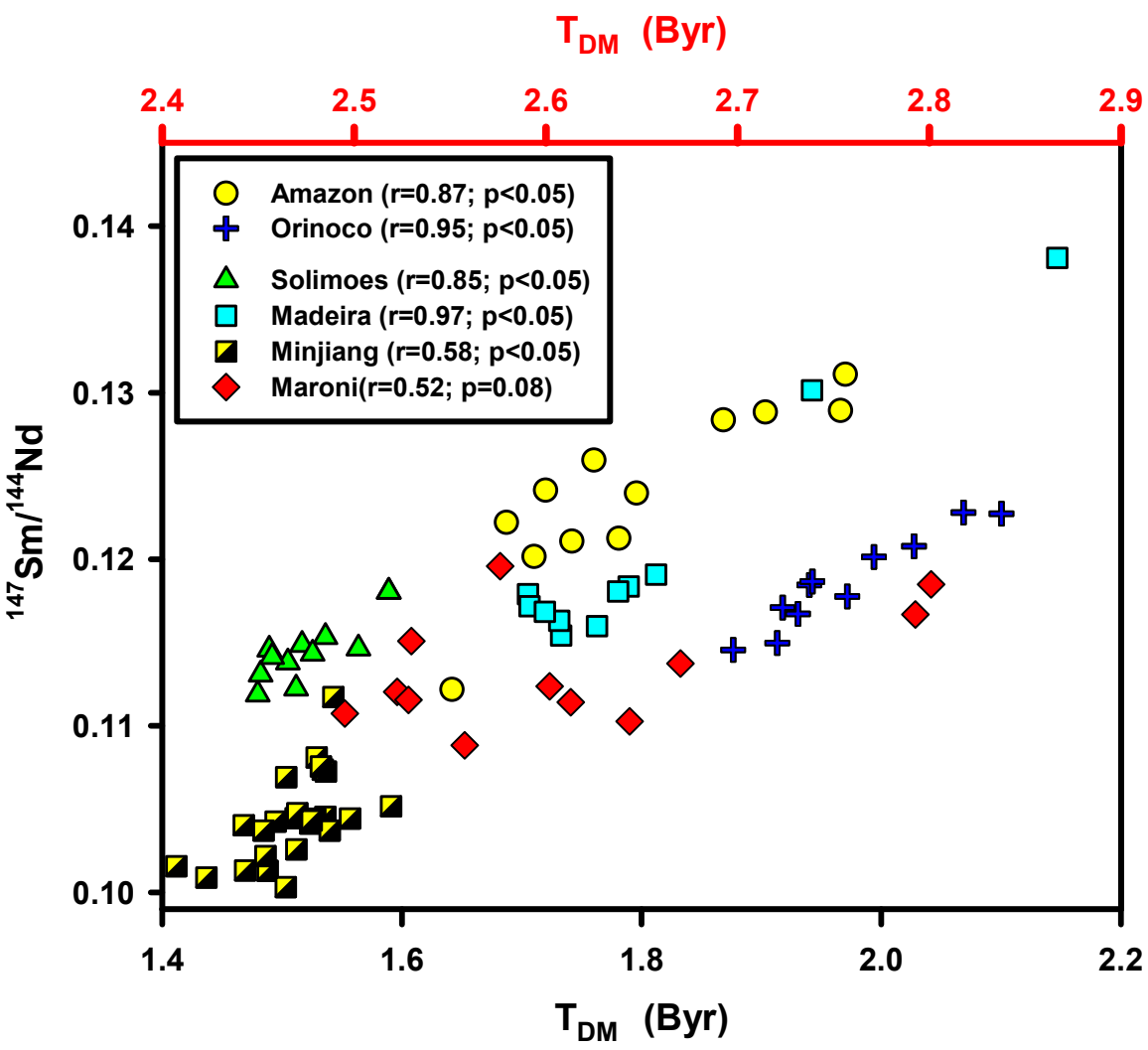

Fig. 8. Time-series data of river particulate ε_{Nd} values are not influenced by age and composition of source rocks. The depleted mantle model ages (T_{DM}) of the SPM were determined as $T_{DM} = \frac{1}{\lambda_{Sm}} \ln\left[\frac{\left(\frac{^{143}Nd}{^{144}Nd}\right)_{sample} - \left(\frac{^{143}Nd}{^{144}Nd}\right)_{DM}}{\left(\frac{^{147}Sm}{^{144}Nd}\right)_{sample} - \left(\frac{^{147}Sm}{^{144}Nd}\right)_{DM}} + 1\right]$ where λ_{Sm} is the decay constant of ^{147}Sm (6.54×10^{-12} y^{-1}), $(^{143}Nd/^{144}Nd)_{DM}$ and $(^{147}Sm/^{144}Nd)_{DM}$ of the present day depleted mantle are 0.513155 and 0.21378, respectively (Goldstein et al., 1984). An inverse correlation is expected if the particulate ε_{Nd} values are significantly influenced by the model age and composition of source rocks. In contrast, significant positive correlations are observed, thus indicating the dominant influence of weathering and riverine transport on particulate Sm/Nd and ε_{Nd} values. Note that T_{DM} values of the Maroni River SPM are plotted against the upper horizontal scale. Data sources: Amazon (Rousseau et al., 2019), Orinoco (Rousseau et al., 2019), Maroni (Rousseau et al., 2019), Solimoes (Viers et al., 2008), Madeira (Viers et al., 2008) and Minjiang River (Jian et al., 2020a; 2020b).

Supplementary information for

Incongruent chemical weathering and adsorption of neodymium drive modulation of neodymium isotope composition of global riverine particulate matter

Anup Kumar Sharma[1], Tarun Kumar Dalai[1], Prem Chand Kisku[2], Jitendra Kumar Pattanaik[3], Sambuddha Misra[4], Shivansh Verma[5], Anil Dutt Shukla[5,6]

[1]Department of Earth Sciences, Indian Institute of Science Education and Research Kolkata, Mohanpur 741246, India

[2]Council of Scientific and Industrial Research-National Geophysical Research Institute (CSIR-NGRI), Uppal Road, Hyderabad 500007, India

[3]Department of Geology, Central University of Punjab, Bathinda, Punjab 151401, India

[4]Centre for Earth Sciences, Indian Institute of Science, Bangalore 560012, India

[5]Geosciences Division, Physical Research Laboratory, Ahmedabad 380009, India

[6]Department of Geology, HNB Garhwal University, Srinagar, Uttarakhand 246174, India

The Supplementary information include:

1. **Supplementary Note SN1:** The study area.
2. **Supplementary Note SN2:** Assessment of preservation of weathering profiles and possible aeolian contributions
3. **Supplementary Note SN3:** Loss of Nd during chemical weathering.
4. **Supplementary Note SN4:** Determination of ε_{Nd} of the residual phases.
5. **Supplementary Note SN5:** Time-series and seasonal data on global riverine particulate ε_{Nd}.
6. **Supplementary Note SN6:** Averaging of discharge and particulate ε_{Nd} of the time-series data
7. **Supplementary Note SN7:** Modelling the impact of Nd adsorption vis-a-vis ε_{Nd} difference between the river water and particulate phase on the seasonal variation of the particulate ε_{Nd}.
8. **Supplementary Figures:** Figure SF1 to Figure SF9.
9. **Supplementary Table ST1:** Major, trace element and Nd isotope composition of weathering profiles.
10. **Supplementary Table ST2:** Immobile elemental ratios of parent basalts and weathering profiles.
11. **Supplementary Table ST3:** The composition of the extracted oxyhydroxide and exchangeable phases. The calculated ε_{Nd} values of the residual phases and the ε_{Nd} difference between the parent basalt and residual phases are also given.
12. **Supplementary Table ST4:** Mean particulate ε_{Nd} values of global rivers during low and high discharge periods.
13. **Supplementary Table ST5:** Results of regression analysis of particulate ε_{Nd} vs. discharge of time series data.

Supplementary Note SN1: The Study area

The Rajmahal Volcanic Province (RVP) covers an area of about 4300 km^2 and comprises mainly of basalts and inter-trappean beds (Ghose et al., 2017). The RVP is bounded by the Precambrian Chotanagpur Gneissic complex (CGS**)** in the southwest and the Quaternary alluvium of the Bengal Basin in the east (Supplementary Fig. SF1). The Gondwana Supergroup overlies the CGS and is underlain by the Rajmahal flood basalts (Ghose et al., 2017).

The Rajmahal basalts have been dated at 118±2 Myr (Ghose et al., 2017). The rocks are primarily tholeiitic basalts and basaltic andesites, with minor abundance of trachyandesites, andesites, dacites, and rhyolites. The basalts are made up of labradoritic plagioclase, pigeonitic-augitic pyroxene, opaque minerals and primary glass (Mukherjee, 1971). The region experiences today a humid to sub-humid climate, and receives an average annual rainfall of about 1550 mm mostly via southwest monsoon circulation. Major rivers flowing through the terrain are Gumani, Brahmani and Bansloi River (Supplementary Fig. SF1).

Two weathering profiles, namely the Dalahi and Pakuria, were collected from the southern part of the Rajmahal trap in the state of Jharkhand (Supplementary Fig. SF1). The RVP is characterized by the development of laterites in the eastern part of the province (Ghosh and Guchhait, 2019). These laterites are characterized by CIA values >99 and are presumed to be of Eocene-Miocene in age based on presence of the dicotyledonous and angiospermous fossil woods (Ghosh et al., 2015; Ghosh and Guchhait, 2019). While ferricretes and laterites have been reported in Pakur district (Ghosh et al., 2015), the concentration of Al is <11 % in both the profiles, thus clearly indicating that the leaching of the elements are only moderate. Such an inference is further supported by progressive upward increase of CIA values, with the maximum values in the range of 75 to 79 in the two studied profiles. We therefore contend that weathering

history of these profiles is much younger, relative to the inferred age of the primary laterites (Ghosh et al., 2015). The top sample of the Pakuria profile and top two samples of the Dalahi profile depict abnormal variation trends in the mineralogical and elemental composition (see Supplementary Note SN2 for a detailed assessment).

The Dalahi profile (DP) is exposed along the southern wall of a stone quarry near the Dalahi village of Dumka district (24° 13.12' N, 87° 38.76' E; Supplementary Fig. SF1). At ~50 cm from the surface, ferricrete nodules are observed and traces of these nodules persist up to a depth of about 90 cm. Saprolites of varying degrees of weathering were observed. Eleven samples were collected from the upper ~200 cm of the profile. The basalt samples (RJS 12 to 16) were collected from a ~1.5 m section of an open pit mine situated within ~50 cm of the profile. The Pakuria profile (PP) is developed near Pakuria village of the Pakur district (24° 18.26' N, 87° 45.30' E; Supplementary Fig. SF1). This profile was sampled from a well exposed section in a stone quarry. The total exposed depth of the profile was more than 15 meters. The horizon within the upper 70 cm was characterized by reddish-brown color and medium to coarse grain ferricrete nodules. The ongoing weathering is evident from the presence of mixture of saprolites and mineral fragments between 70 to 625 cm depth of the profile. The top 50 cm was not sampled to avoid the plant roots and contamination from overburden materials. Nine samples were collected from the profile. The fresh basalt sample (PFB1) was obtained at a depth of 10 meters.

Supplementary Note SN2: Assessment of preservation of weathering profiles and possible aeolian contributions

The preservation and *in-situ* nature of the weathering profile was evaluated using data on major and trace element compositions (Supplementary Table ST1). The Si/Al ratios exhibit a general decrease and the CIA values increase from the parent rock towards the top of the profile, with the

1175 exception of top two samples in DP and the topmost sample in PP (Supplementary Fig. SF2).
1176 Therefore, elemental compositions clearly document progressive weathering of basaltic rocks,
1177 indicating well preservation of the profiles. The unusual increase of Si/Al ratios in the top two
1178 samples of DP and one sample of PP is presumably due to external influences such as lateral
1179 transport.

1180 The *in-situ* nature and preservation of weathering profiles is routinely assessed by using
1181 immobile element ratios (Maynard, 1992; Nesbitt and Markovics, 1997). The robustness of these
1182 ratios is due to their limited variation during weathering and transport, although their absolute
1183 elemental concentrations could show a considerable scatter. However, the characteristic narrow
1184 range of variation can be violated by mixing with materials external to the weathering profile.
1185 We use two such ratios (Nb/Al and Th/Al) to evaluate the *in-situ* nature of the profiles
1186 (Supplementary Table ST2, Supplementary Fig. SF2). With the exception of top two samples of
1187 DP and the topmost sample of PP, the mean of the elemental ratios agree within uncertainties
1188 with the ratios measured for the parent basalts. Therefore, the ratios of immobile elemental
1189 concentrations firmly establish the well-preserved and in-situ nature of the two profiles. The
1190 trace element ratios of topmost two samples of DP and one sample of PP (Supplementary Table
1191 ST2, Supplementary Fig. SF2) are outside the range of the values for the rest of the profile and
1192 the parent rocks. Therefore, based on collective evidence of the mineral, major element and
1193 immobile trace element composition, we infer that the topmost sections (shaded portion in
1194 Supplementary Fig. SF2) are influenced by lateral transport. Therefore, we exclude data of these
1195 samples from further evaluation and discussion.

1196 The excellent agreement of the immobile element ratios between the parent basalts and
1197 weathering profile samples also indicates the aeolian contributions to be insignificant. We

corroborate such an assessment through three immobile elements (La-Th-Sc) discrimination diagram that is routinely employed to determine source compositions (Wang et al., 2018; Yuan et al., 2022). It is evident (Supplementary Fig. SF3) that the immobile element compositions of the weathering profiles are distinctly different than those of the potential dust sources, but nearly identical to those of the parent basalts. These observations confirm our contention that the two studied profiles are not contaminated by aeolian contributions.

Supplementary Note SN3: Loss of Nd during chemical weathering

The percentage loss of Nd from the weathering profiles were determined as follows:

$$[Nd]_{lost}\ \% = \left[1 - \left(\frac{\left[\frac{Nd}{Th}\right]_{bulk}}{\left[\frac{Nd}{Th}\right]_{p}}\right)\right] \times 100 \qquad \text{Eq (1)}$$

where subscripts *bulk* and *P* refer to the [Nd] in the bulk weathered materials and parent basalts, respectively. Th is used as a normalizing element due to its immobile behavior during the chemical weathering of basalts (Ma et al., 2007).

Supplementary Note SN4: Determination of ε_{Nd} of the residual phases

The ε_{Nd} values of the residual phases were calculated based on the premise that the bulk materials of the profiles are composed of the residual products and components adsorbed from the weathering solutions onto the oxyhydroxide phases. The ε_{Nd} of the adsorbed components was considered to be the same as measured on oxyhydroxides phases. Mass balance relations for the Nd and ε_{Nd} are:

$$f_{Nd}^{Res} = 1 - \left(\frac{[Nd]_{ads}}{[Nd]_{bulk}}\right) = 1 - \left(\frac{[Nd]_{ox}}{[Nd]_{bulk}}\right) \qquad \text{Eq. (2)}$$

$$f_{Nd}^{ox} = \frac{[Nd]_{ox}}{[Nd]_{bulk}} \qquad \text{Eq. (3)}$$

$$\varepsilon_{Nd}^{bulk} = f_{Nd}^{Res} \times \varepsilon_{Nd}^{Res} + f_{Nd}^{ox} \times \varepsilon_{Nd}^{ox} \quad \text{Eq. (4)}$$

where f_{Nd} denotes the fraction of Nd in the bulk phase, and the terms *ads*, *Res* and *ox* refer to residual and oxyhydroxides, respectively. The ε_{Nd} values of adsorbed and residual component are calculated as:

$$\varepsilon_{Nd}^{ads} = \varepsilon_{Nd}^{ox} \quad \text{Eq. (5)}$$

$$\varepsilon_{Nd}^{Res} = \left(\frac{\varepsilon_{Nd}^{bulk} - [f_{Nd}^{ox} \times \varepsilon_{Nd}^{ox}]}{f_{Nd}^{Res}} \right) \quad \text{Eq. (6)}$$

The values of ε_{Nd}^{ox} and ε_{Nd}^{Res} are listed in supplementary Table ST3.

Supplementary Note SN5: Time-series and seasonal data on global riverine particulate ε_{Nd}

The time-series data of rivers evaluated in this study are from existing literature and cover at least one full annual discharge cycle for Amazon, Orinoco, Madeira, Solimoes, Maroni, Tumbes, Minjiang and Changjiang (Supplementary Table ST4). The discrete seasonal ε_{Nd} data represent the dry and wet periods for the rivers Ganga, Brahmaputra, Amazon, Changjiang, Uruguay, Tapajos, Parana, and Xingu. However, these data do not represent the maximum and minimum flow conditions of an annual discharge cycle. The discharge (Q) and SPM concentration data for the Minjiang River (Jian et al., 2020b) were obtained from figures using PlotDigitizer software that has been reported to extract data reliably (Aydin and Yassikaya, 2021).

With the exception of the Changjiang data at Nanjing, eight sets of time-series data representing seven rivers individually demonstrate clear inverse ε_{Nd}–Q relationships (Supplementary Table ST5). The ε_{Nd} data of the Changjiang River SPM were measured after leaching the bulk SPM with 0.5 M acetic acid (Mao et al., 2011) The amorphous Fe-Mn oxyhydroxides are soluble, albeit sparingly, in acetic acid (Tachambalath et al., 2023). Therefore, it is unclear how and to what degree Nd hosted by amorphous oxyhydroxides may have been

impacted by acid leaching. Furthermore, after the construction of the Three Gorges Dam, increased channel erosion in the lower reaches has been reported to contribute more unradiogenic Nd in the dry seasons (Mao et al., 2011). Although the variation of ε_{Nd} with discharge has been explained in terms of variable contributions of sediments from upper and lower reaches of river (Mao et al., 2011), the lack of data on [Nd] does not allow us to test if mixing is responsible for the observed ε_{Nd}–Q relationship. The idea that the dissolved phase of this river could have been less radiogenic than the SPM is not supported by the discrete seasonal data available at Datong (Luo et al., 2012) which show a higher particulate ε_{Nd} in the low discharge period (Supplementary Table ST4). We therefore contend that further studies of time-series data of coexisting dissolved-SPM phases both the in the upper and lower reaches are required for a reliable evaluation of the processes regulating the seasonal variation of particulate ε_{Nd} of the Changjiang River.

In the discrete-seasonal datasets, six of the eight rivers are characterized by higher particulate ε_{Nd} in the low discharge periods, which is supportive of our framework of interpretation. While the discrete low-resolution data could be biased by unusual and extreme fluctuations, the following circumstantial evidence supports the seasonal trend of particulate ε_{Nd} data for the Ganga and Brahmaputra Rivers. The dissolved phase of the Ganga River has been reported to have higher ε_{Nd} than the coexisting SPM (Chatterjee and Singh, 2014). In addition, the study of Galy et al. (1998) reported that the clay fractions of the Ganga and Brahmaputra rivers, bearing a greater potential for Nd adsorption, have ε_{Nd} values up to 3 units higher than the bedload samples.

The discrete seasonal data of three rivers (Amazon, Tapajos and Xingu) are characterized by low precision for the particulate ε_{Nd} ($\pm 2\sigma$ = 0.14 to 0.39). Out of these, one river shows

negative values of $\Delta\varepsilon_{Nd}^{LQ\text{-}HQ}$. However, owing to large uncertainties, the $\Delta\varepsilon_{Nd}^{LQ\text{-}HQ}$ values are indistinguishable from zero.

Supplementary Note SN6: Averaging of discharge and particulate ε_{Nd} of the time-series data

In order to minimize the bias due to extreme fluctuations, the seasonal averaging of discharge and ε_{Nd} of the time-series data were performed after excluding the distinct outliers (Supplementary Table ST4). The scheme of data averaging depended on the discharge contrast between seasons and temporal resolution of available ε_{Nd} data in a given flow period. Such a scheme involved averaging data of samples representing ~35% and ~15% of the lowest and highest discharge, respectively. Two to six data points were used to calculate the means for both the low and high flow periods (ε_{Nd}^{LQ} and ε_{Nd}^{HQ}). However, for the river Minjiang, no averaging could be done for the high flow period due to lack of enough ε_{Nd} data. The errors of average ε_{Nd} values (Supplementary Table ST4) are determined from the reported uncertainties in the literature.

Supplementary Note SN7: Modelling the impact of Nd adsorption vis-a-vis ε_{Nd} difference between the river water and particulate phase on the seasonal variation of the particulate ε_{Nd}

We utilized a mass balance model to elucidate the impact of adsorption on ε_{Nd} of SPM during peak and lean flow periods. The model was constructed based on the assumption that prior to Nd adsorption in rivers, ε_{Nd} of SPM ($\varepsilon_{Nd}^{SPM_o}$), and ε_{Nd} of the river water (ε_{Nd}^{Riv}) are the same during the peak and lean flow periods.

For the peak flow period:

$$\varepsilon_{Nd}^{HQ} = f_{Nd}^{HQ} \times \varepsilon_{Nd}^{Riv} + (1 - f_{Nd}^{HQ}) \times \varepsilon_{Nd}^{SPM_o} \quad \text{Eq. (7)}$$

For the lean flow period:

$$\varepsilon_{Nd}^{LQ} = f_{Nd}^{LQ} \times \varepsilon_{Nd}^{Riv} + (1 - f_{Nd}^{LQ}) \times \varepsilon_{Nd}^{SPM_o} \quad \text{Eq. (8)}$$

where f_{Nd} denotes the fraction of Nd adsorbed onto the riverine SPM, and ε_{Nd}^{HQ} and ε_{Nd}^{HQ} represent the Nd isotopic composition of the riverine SPM after Nd adsorption during the high flow and low flow periods, respectively.

From eq. (7) and (8), we get

$$(\varepsilon_{Nd}^{LQ} - \varepsilon_{Nd}^{HQ}) = (f_{Nd}^{LQ} - f_{Nd}^{HQ}) \times (\varepsilon_{Nd}^{Riv} - \varepsilon_{Nd}^{SPM_o}) \quad \text{Eq. (9)}$$

Therefore,

$$\Delta\varepsilon_{Nd}^{LQ-H} = \Delta f_{Nd}^{LQ\text{-}HQ} \times \Delta\varepsilon_{Nd}^{Riv\text{-}SPM_o} \quad \text{Eq. (10)}$$

The expression (Eq. 10) clearly demonstrates that seasonal difference of adsorbed Nd fractions and ε_{Nd} difference between the river water and SPM prior to adsorption, together influence $\Delta\varepsilon_{Nd}^{LQ\text{-}HQ}$ (cf. Supplementary Fig. SF4).

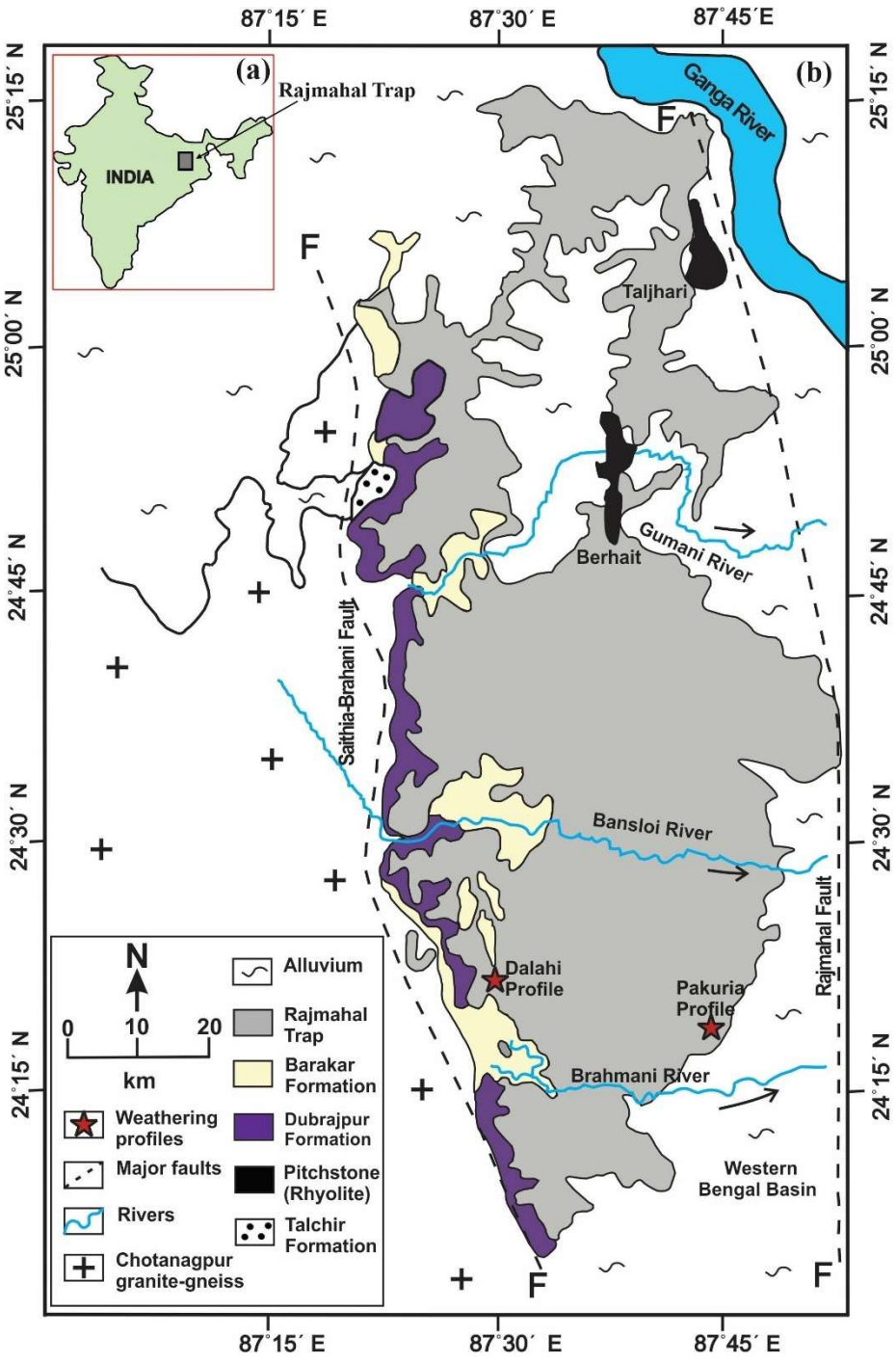

Supplementary Fig. SF1. The study area and weathering profiles. **(a)** The trap basalts of the Rajmahal Volcanic Province in India. **(b)** Geological map of the Rajmahal Volcanic Province (modified after Ghose et al. 2017), showing the areal extent of trap basalts and location of the studied weathering profiles (red stars). The formations of the Gondwana Supergroup (Dubrajpur, Barakar and Talchir formations) and Chotanagpur granite-gneiss are also shown.

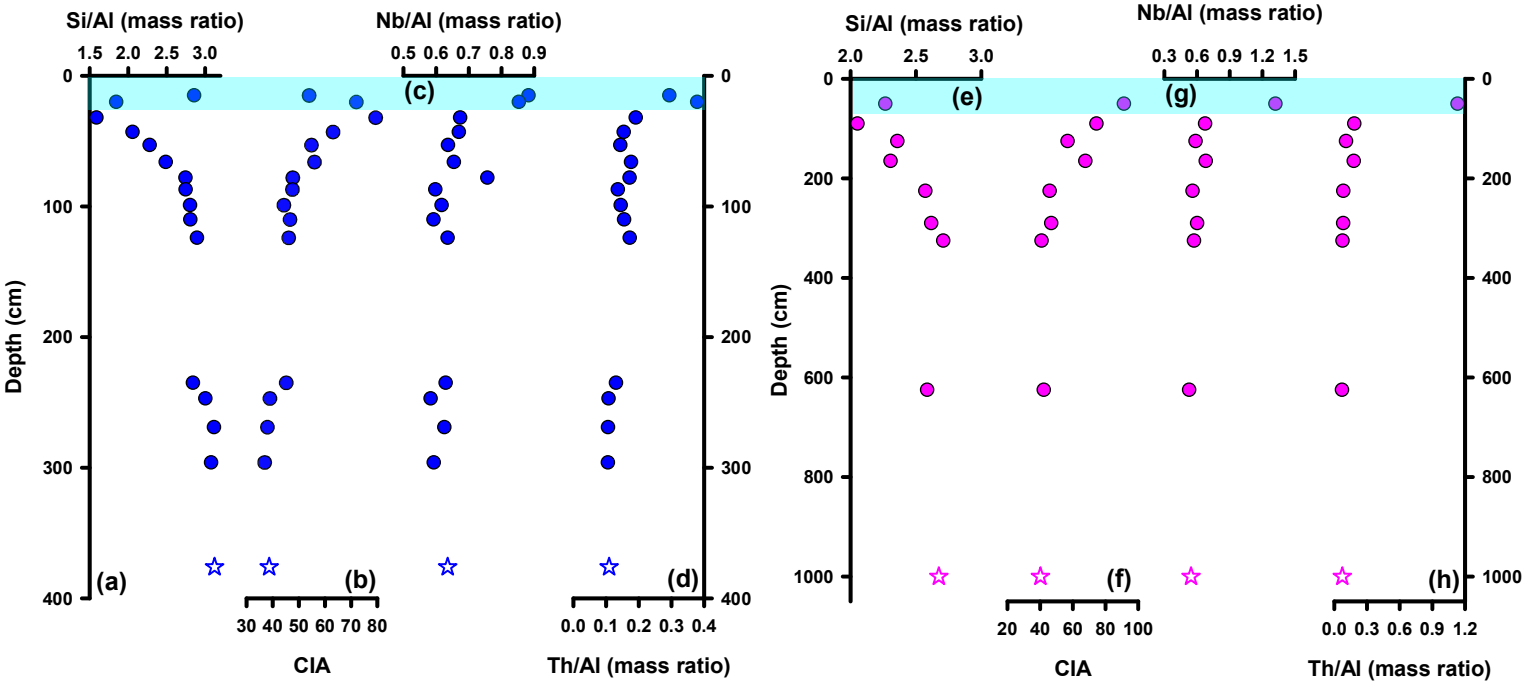

Supplementary Fig. SF2. Progressive weathering and preservation of weathering profiles. **(a, b, e, f):** Upward decrease of Si/Al and increase of CIA indicate progressive weathering towards the top. **(c, d, g, h):** Variation of immobile element ratios (Nb/Al and Th/Al) in the weathered-materials and parent basalts (stars). Comparable ratios between the parent basalts and the weathered-materials attest to the *in-situ* characteristics of the profiles. The shaded top portions are inferred to be contaminated by lateral transport, as evident from Nb/Al and Th/Al ratios that are very different compared to parent basalts (See Supplementary Note SN2 for the detailed discussion). Dalahi profile: blue, Pakuria profile: pink.

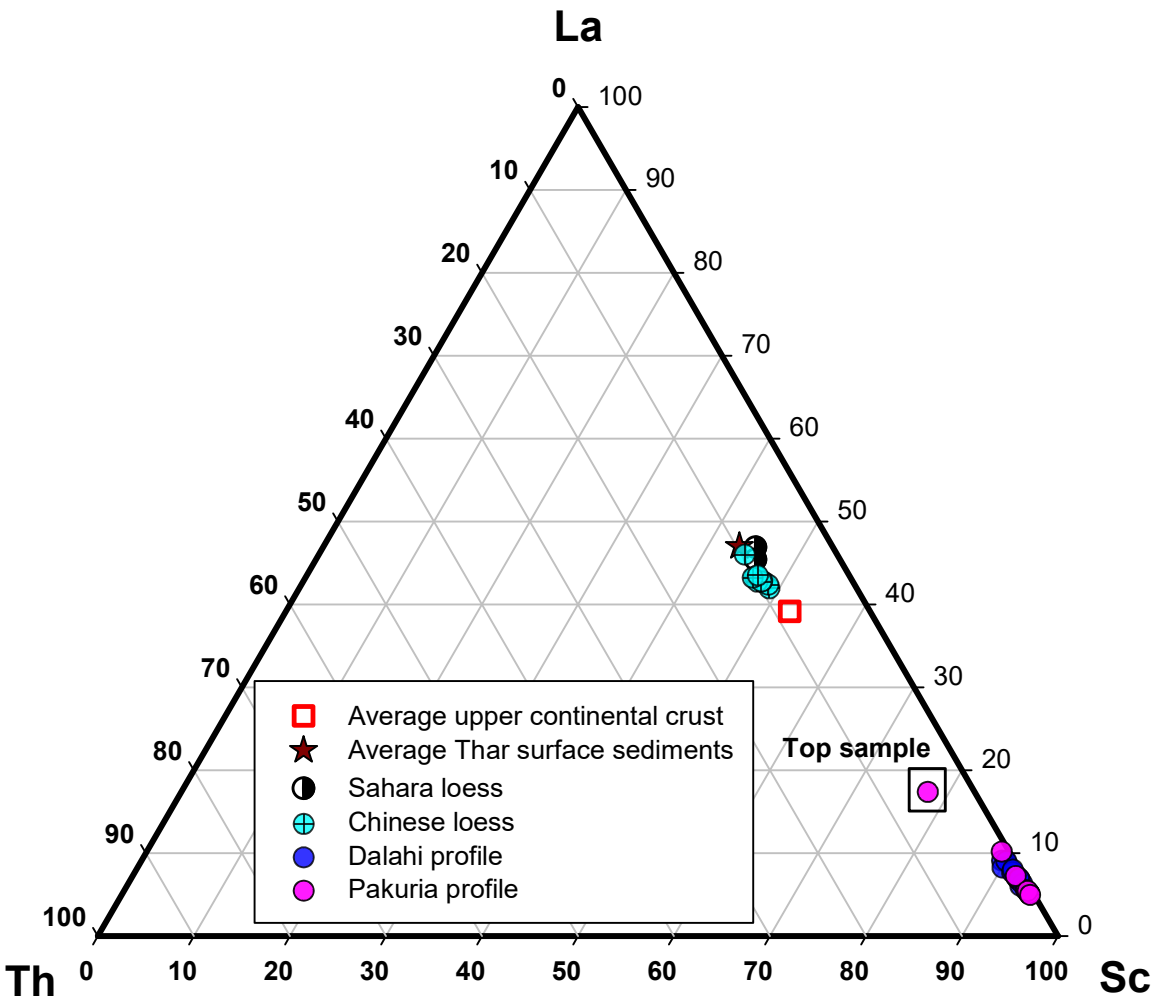

Supplementary Fig. SF3. The La–Th–Sc discrimination diagram comparing the distributions of immobile elements in the two basaltic weathering profiles (including the parent basalts) with those in the average upper continental crust (Taylor and McLennan, 1985), and the primary sources of aeolian dust in Asia: Thar desert surface sample (Bhattacharyya et al., 2024), and loess from China (Wang et al., 2018) and the Sahara (Chauvel et al., 2014). The weathering profile samples have distinctly different compositions compared to the potential dust sources. The concentrations data for the weathering profiles are given in supplementary table ST1.

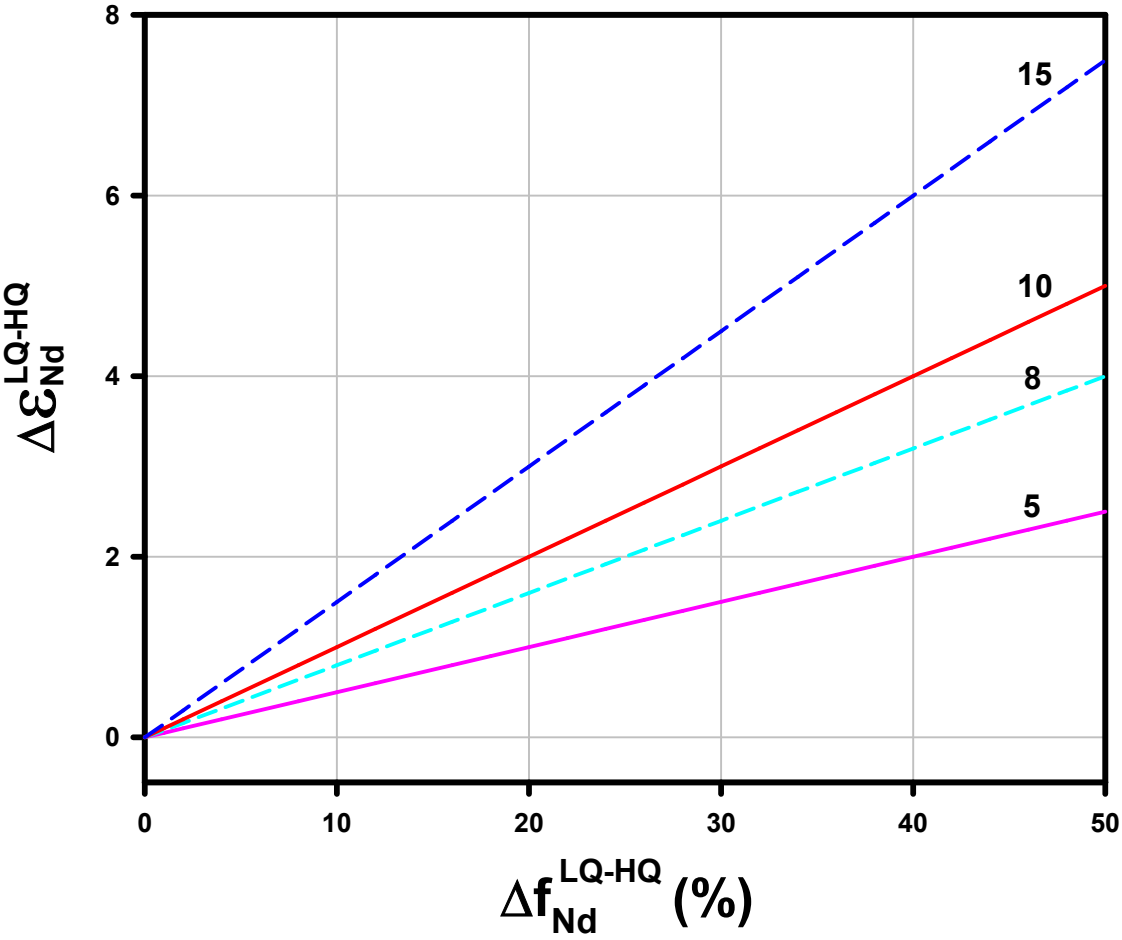

Supplementary Fig. SF4. Combined impact of Nd adsorption and $\Delta\varepsilon_{Nd}^{Riv-}$ ° on $\Delta\varepsilon_{Nd}^{LQ-HQ}$. Variation of $\Delta\varepsilon_{Nd}^{LQ\text{-}HQ}$ as a function of difference in the degree of Nd adsorption and difference of ε_{Nd} between dissolved phase and SPM. The lines correspond to variable values of $\Delta\varepsilon_{Nd}^{Riv-SPM_o}$. The choice of $\Delta\varepsilon_{Nd}^{Riv-SPM_o}$ were based on the reported $\Delta\varepsilon_{Nd}^{Riv-SPM}$ of ~5 (Hindshaw et al., 2018b) and ~8 (Larkin et al., 2021), $\Delta\varepsilon_{Nd}^{Leach-Residue}$ of ~4 (Tricca et al., 1999) and 15 (Hindshaw et al., 2018a). See Supplementary Note SN7 for the mass balance model developed to elucidate the influence of Δf_{Nd}^{LQ-HQ} and $\Delta\varepsilon_{Nd}^{Riv-SPM_o}$ on $\Delta\varepsilon_{Nd}^{LQ\text{-}HQ}$.

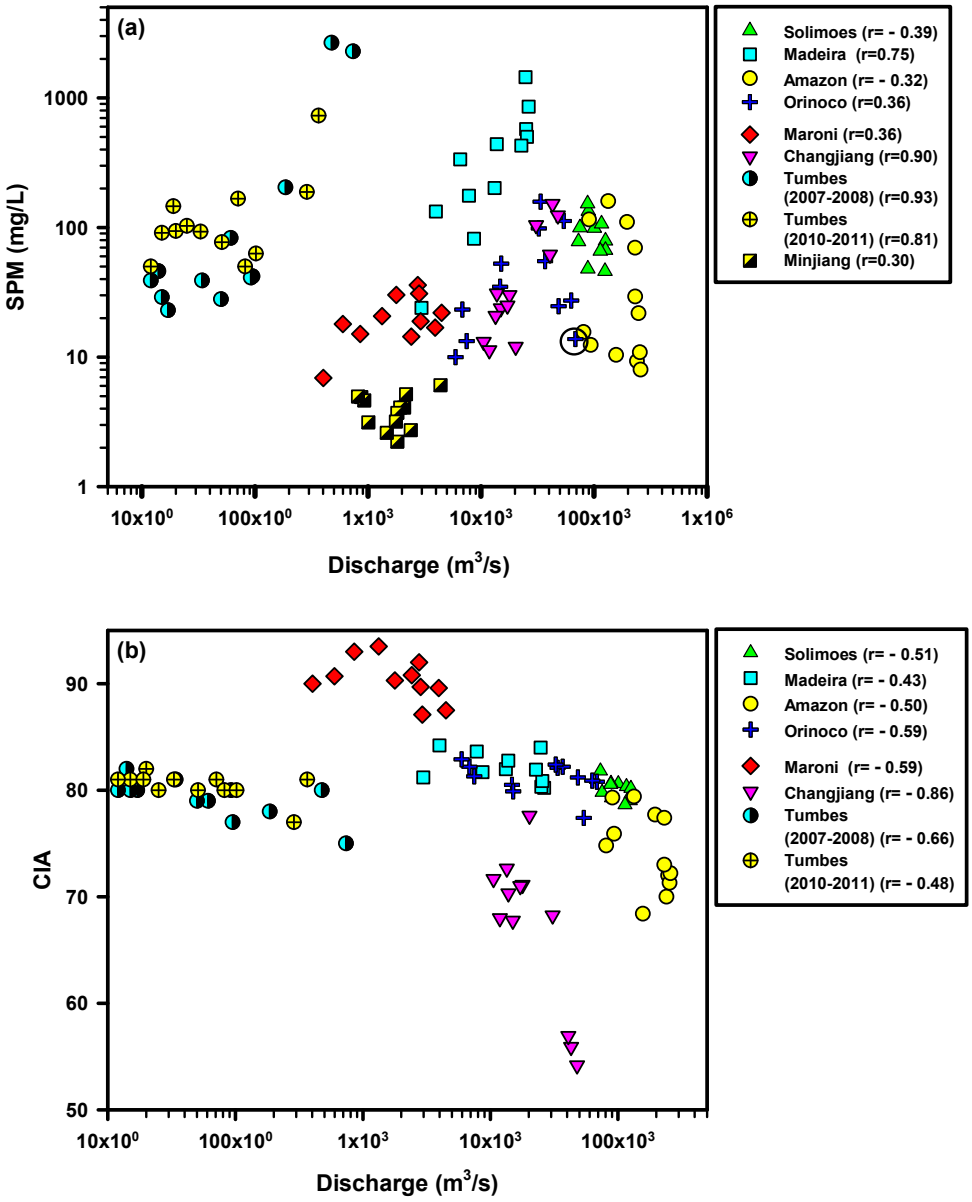

Supplementary Fig. SF5. Variation of [SPM] **(a)** and chemical index of alteration (CIA) **(b)** as a function of river water discharge. **(a)** SPM concentrations are typically higher in the high discharge periods with the exception of the Amazon and Solimoes Rivers, which show the least variation in discharge (Supplementary Table ST4). **(b)** General inverse correlations between CIA and river water discharge indicate a higher degree of chemical weathering and production of secondary minerals in the low flow periods due to longer solid-solution contact time. One outlier (circled) is excluded from regression analysis. Data sources: Amazon (Rousseau et al., 2019), Orinoco (Rousseau et al., 2019), Maroni (Rousseau et al., 2019), Solimoes (Viers et al., 2008), Madeira (Viers et al., 2008), Minjiang (Jian et al., 2020a; 2020b), Tumbes (Moquet et al., 2020) and Changjiang River (Mao et al., 2010). CIA values of the Changjiang River were calculated using major element oxides data sourced from Mao et al. (2010).

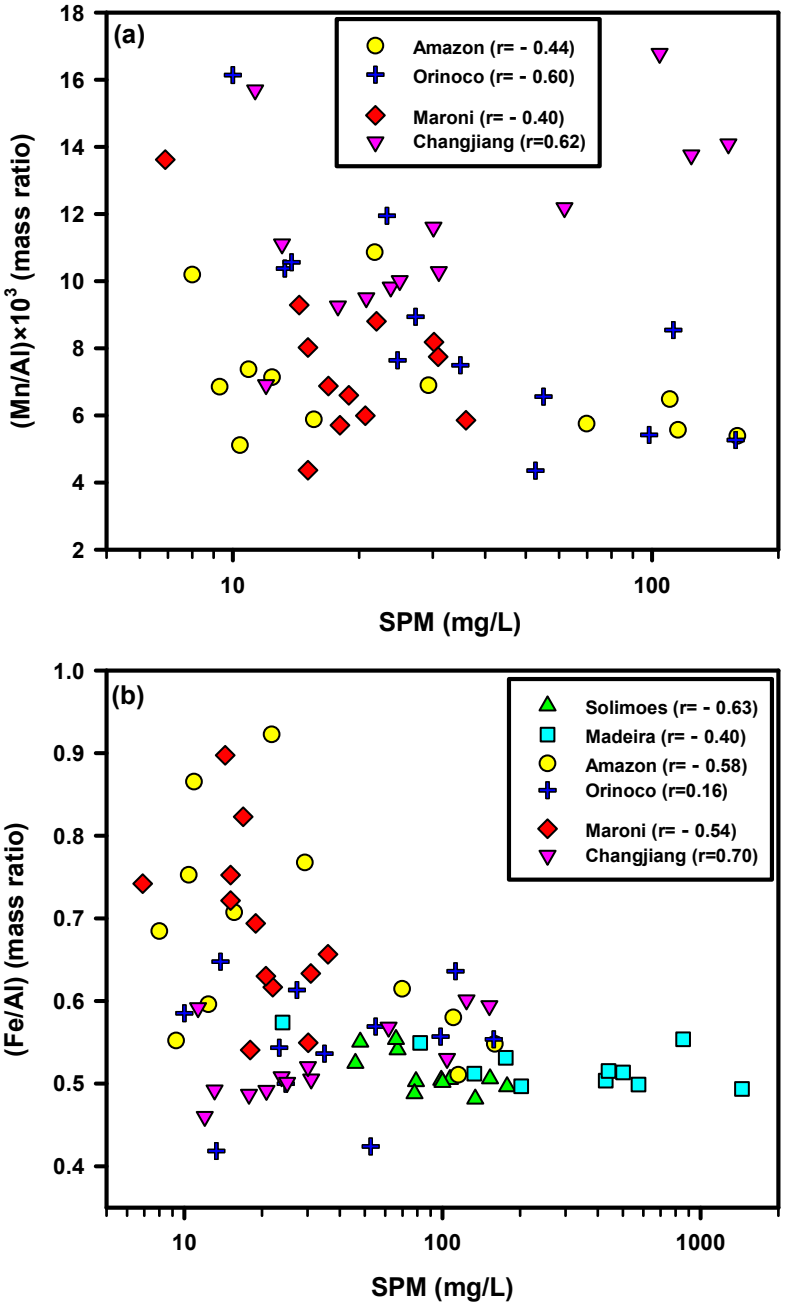

Supplementary Fig. SF6. Abundance of oxyhydroxide phases as a function of SPM concentrations. Inverse correlations of Fe/Al and Mn/Al ratios with SPM concentrations are apparent for all rivers except the Changjiang River. For Orinoco River, no significant correlation is observed between Fe/Al and SPM concentrations. The observations of this figure and Supplementary Fig. SF5 together indicate higher abundances of oxyhydroxide phases (adsorbents) in the low flow periods. Data sources: Amazon (Rousseau et al., 2019), Orinoco (Rousseau et al., 2019), Maroni (Rousseau et al., 2019), Solimoes (Viers et al., 2008), Madeira (Viers et al., 2008) and Changjiang River (Mao et al., 2010).

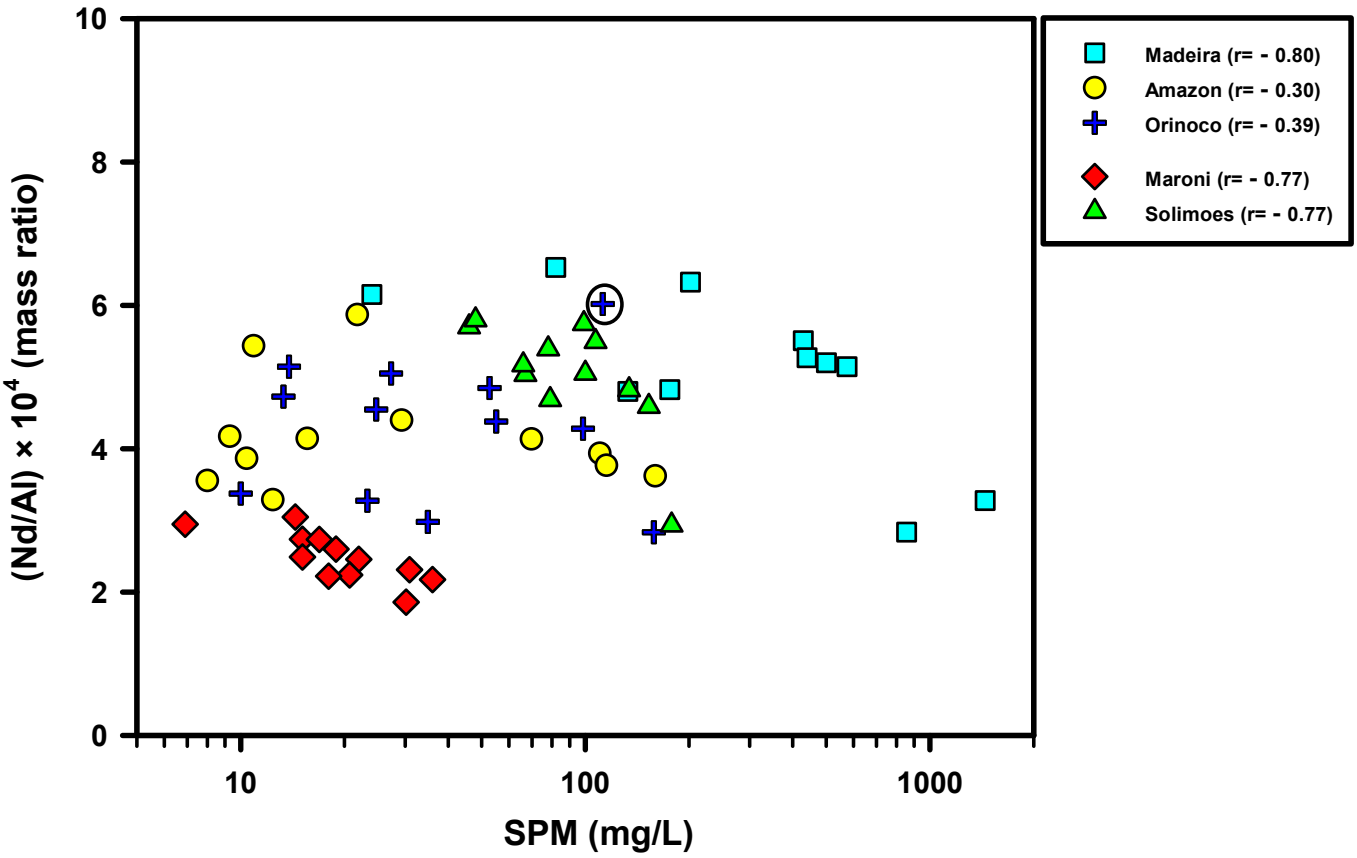

Supplementary Fig. SF7. Nd adsorption as a function of SPM concentrations. General inverse correlations of Nd/Al ratio with SPM concentrations indicate higher degree of Nd adsorption at lower SPM concentrations, which is observed in low flow periods when the oxyhydroxide phase concentrations are relatively higher (cf. Supplementary Fig. SF5-6). One Outlier (circled) is excluded from regression analysis. Data sources: Amazon (Rousseau et al., 2019), Orinoco (Rousseau et al., 2019), Maroni (Rousseau et al., 2019), Solimoes (Viers et al., 2008) and Madeira River (Viers et al., 2008).

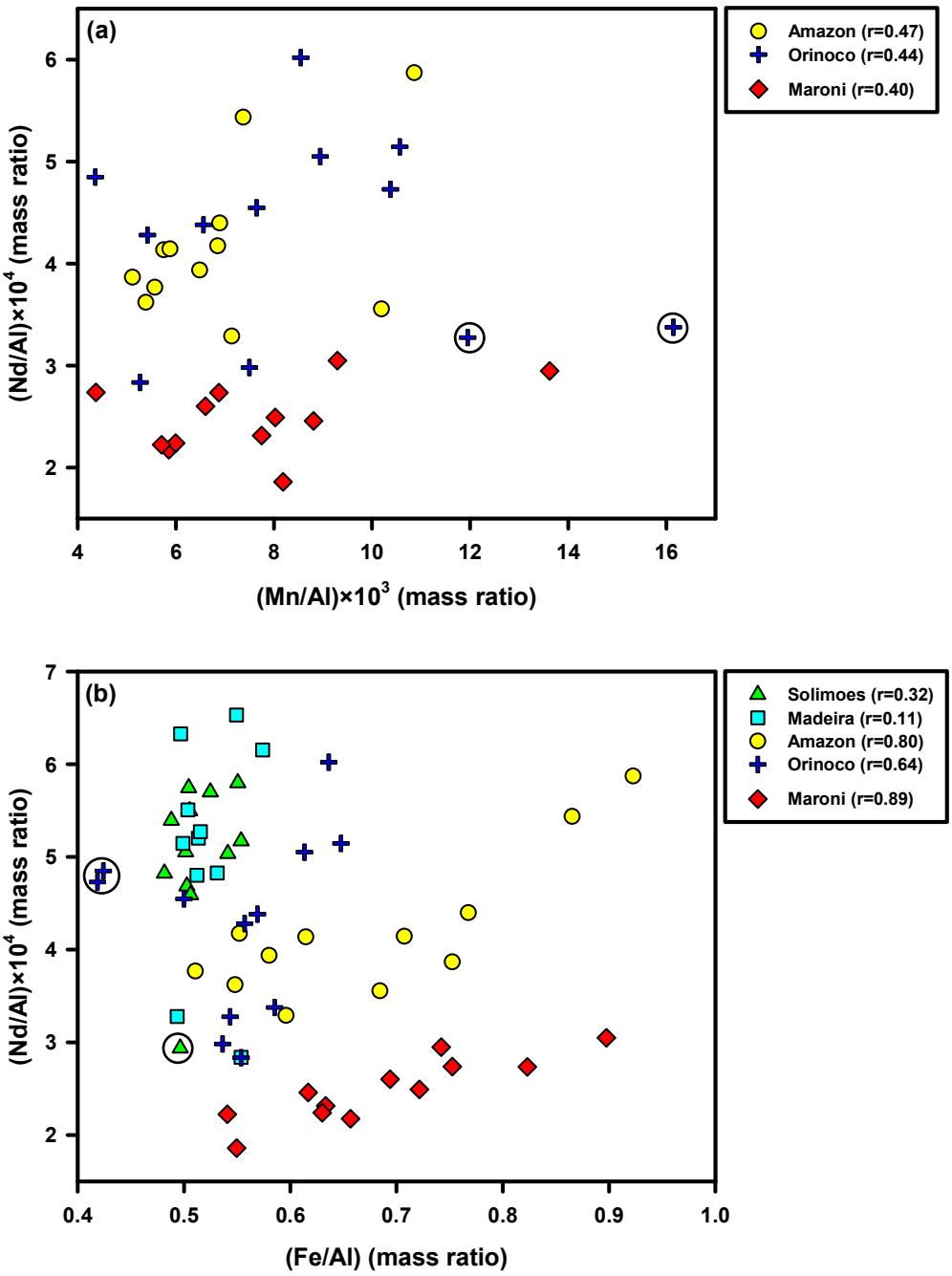

Supplementary Fig. SF8. Nd adsorption as function of abundance of [Fe]-[Mn] oxyhydroxide phases in the SPM. Variation of Nd/Al with the Mn/Al (a) and Fe/Al (b) in the river SPM. Weak to significant positive correlations are observed. The observed variation trends are suggestive of a greater degree of Nd adsorption at higher concentrations of oxyhydroxide phases in the river SPM. Outliers (circled) are excluded from regression analysis. Data sources: Amazon (Rousseau et al., 2019), Orinoco (Rousseau et al., 2019), Maroni (Rousseau et al., 2019), Solimoes (Viers et al., 2008) and Madeira River (Viers et al., 2008).

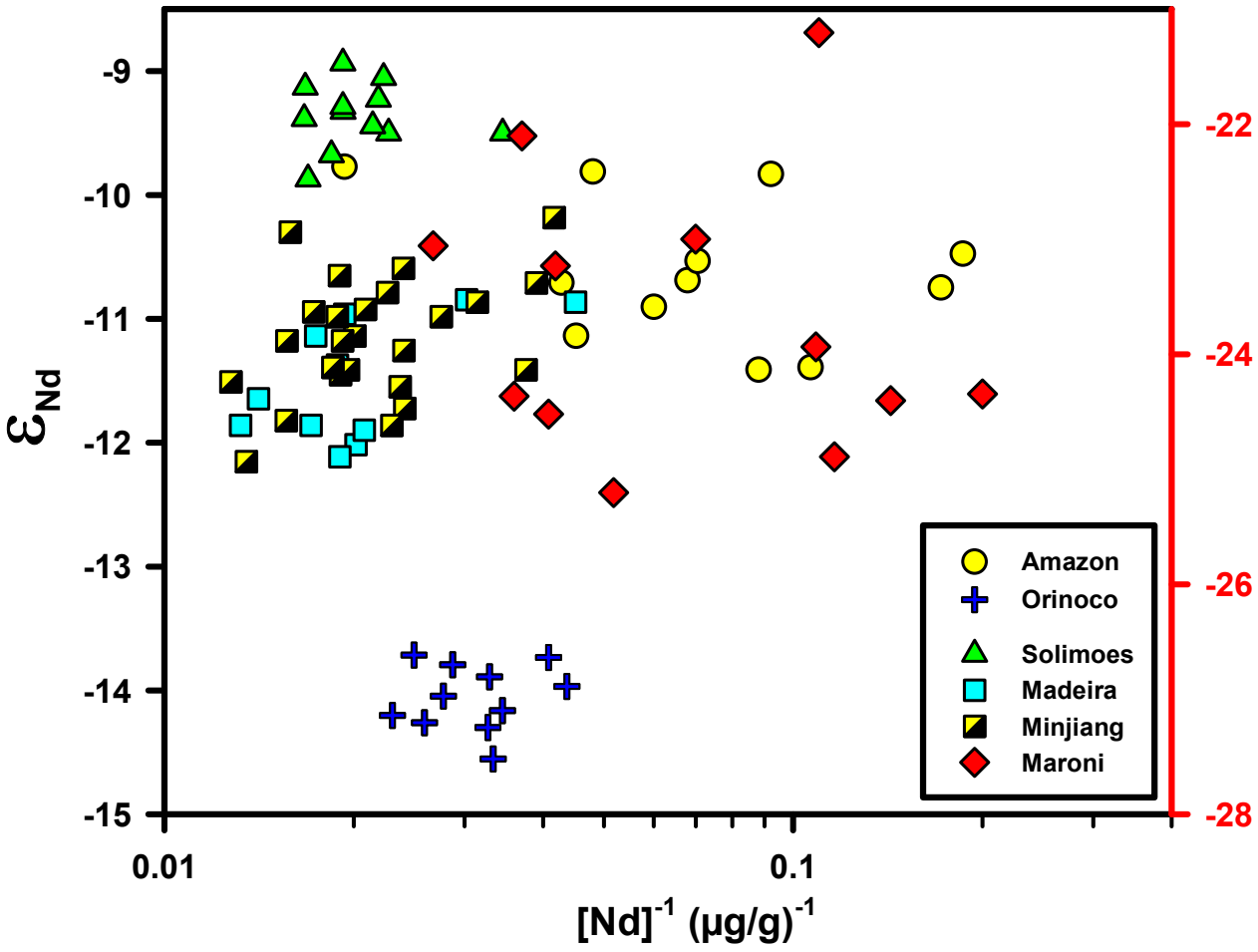

Supplementary Fig. SF9. Evaluation of mixing of source rock contributions to the time-series particulate ε_{Nd} data. Large scatter in the data and a lack of significant linear correlation do not support mixing of variable source rock composition as a driving process for the temporal variation of particulate ε_{Nd} of the global rivers. Note that ε_{Nd} values for Maroni River are plotted against the right-hand side vertical scale. Data sources: Amazon (Rousseau et al., 2019), Orinoco (Rousseau et al., 2019), Maroni (Rousseau et al., 2019), Solimoes (Viers et al., 2008), Madeira (Viers et al., 2008) and Minjiang River (Jian et al., 2020a; 2020b).

Supplementary Table ST1. Major, trace element and Nd isotope composition of weathering profiles.

Sample code	Depth (cm)	Al	Ca	Fe	Mg	Na	K	Si	Mn	CIA*	Nb	Nd	Sm	Sc	La	Th	ε_{Nd}#
		wt. %									µg/g						
Dalahi profile (DP)																	
RJS 1	15	8.25	4.15	10.2	2.27	1.10	0.26	23.6	0.23	54	7.28	17.7	4.70	35.2	11.3	2.42	NA
RJS 2	20	10.2	2.29	12.8	1.48	0.65	0.17	18.7	0.31	72	8.66	21.7	4.50	43.3	12.6	3.85	NA
RJS 3	32	11.2	1.63	14.3	0.96	0.55	0.12	17.8	0.35	79	7.55	21.3	4.52	48.7	10.2	2.14	-1.12
RJS 4	43	9.97	3.40	12.5	1.96	1.01	0.12	20.5	0.35	63	6.67	19.8	4.85	43.6	10.2	1.54	-0.49
RJS 5	53	9.53	4.67	10.1	2.67	1.27	0.12	21.7	0.22	55	6.06	15.8	4.71	39.8	9.48	1.37	-0.03
RJS 6	66	8.98	4.17	10.6	2.42	1.16	0.15	22.3	0.33	56	5.87	18.6	4.94	39.1	10.4	1.58	-0.75
RJS 7	78	8.41	5.43	8.48	2.89	1.52	0.22	23.1	0.26	48	6.36	192	5.44	33.3	10.6	1.45	0.45
RJS 8	87	8.43	5.53	9.05	2.95	1.52	0.13	23.1	0.21	47	5.03	14.4	4.39	35.4	8.81	1.15	0.23
RJS 9	99	8.33	6.27	8.69	3.36	1.68	0.13	23.3	0.18	44	5.13	14.2	4.37	32.8	8.68	1.21	0.74
RJS 10	110	8.35	5.67	9.07	3.00	1.58	0.15	23.5	0.18	47	4.94	13.9	4.25	34.8	8.54	1.30	0.02
RJS 11	124	8.25	5.70	8.53	2.94	1.57	0.19	23.9	0.15	46	5.24	14.1	4.29	31.0	8.32	1.42	-0.11
RJS 12	235	8.30	5.97	8.84	3.17	1.68	0.14	23.6	0.19	45	5.22	14.9	4.61	32.3	9.01	1.09	0.34
RJS 13	247	7.89	7.45	7.98	3.91	1.93	0.14	23.7	0.13	39	4.60	12.6	4.12	31.4	7.19	0.85	1.19
RJS 14	269	7.82	7.63	8.41	3.94	2.05	0.17	24.4	0.14	38	4.89	13.4	4.28	31.9	7.56	0.83	1.86
RJS 15	296	7.76	7.64	8.27	3.91	2.45	0.20	23.9	0.13	37	4.60	12.6	4.06	32.2	6.98	0.82	1.33
RJS 16 (parent)	376	7.70	7.17	8.37	3.83	2.02	0.32	24.0	0.14	39	4.89	13.0	4.23	31.5	7.56	0.84	1.19
Pakuria profile (PP)																	
PA1	50	8.96	0.34	15.8	0.39	0.12	0.38	20.3	0.29	91	11.83	29.8	5.12	32.0	22.4	10.14	NA
PB1	90	9.91	2.02	8.67	1.10	0.47	0.16	20.4	0.19	75	6.70	24.0	6.63	47.8	17.3	1.83	-0.69
PB2	125	9.49	4.15	7.31	1.60	1.25	0.22	22.4	0.11	57	5.57	13.0	4.03	42.5	8.06	1.04	0.76
PB3	165	9.17	2.49	8.55	1.23	0.75	0.20	21.1	0.19	68	6.24	18.4	4.94	44.0	11.1	1.65	-1.04
PB4	225	9.00	6.13	7.46	2.25	1.84	0.28	23.2	0.12	46	5.04	12.0	4.01	40.5	7.14	0.75	1.79
PB5	290	8.76	5.81	7.76	2.15	1.67	0.22	22.9	0.10	47	5.27	12.7	4.09	40.7	7.08	0.72	1.81
PERN	325	8.67	7.14	7.46	2.44	2.31	0.27	23.5	0.12	41	4.97	11.9	3.81	37.0	6.49	0.66	2.03
PFAA	625	9.30	7.00	6.59	2.23	2.58	0.34	24.0	0.10	42	4.92	12.3	4.00	36.7	6.83	0.67	2.17
PFB1 (parent)	1000	8.71	7.40	7.40	2.85	2.42	0.22	23.3	0.12	40	4.75	11.9	3.79	37.8	6.42	0.65	2.45

*CIA values were calculated using the molar proportions of the oxides. CIA = $[Al_2O_3/(Al_2O_3 + CaO + Na_2O + K_2O)] \times 100$.

#$\varepsilon_{Nd} = [\{(^{143}Nd/^{144}Nd)_{sample}/(^{143}Nd/^{144}Nd)_{CHUR}\}-1]\times 10^4$, where $(^{143}Nd/^{144}Nd)_{CHUR} = 0.512638$ (Jacobsen and Wasserburg, 1980).

Supplementary Table ST2. Immobile elemental ratios of parent basalts and weathering profiles.

Profile	Sample code	Nb/Al (mass ratio)	Th/Al (mass ratio)
Dalahi	RJS 1-2	0.85-0.88	0.29-0.38
	RJS 3-15	0.64±0.04	0.14±0.03
	RJS 16 (parent)	0.64	0.11
Pakuria	PA1	1.32	1.13
	PB1-PFAA	0.59±0.06	0.11±0.05
	PFB1 (parent)	0.54	0.07

The codes, depth in the profiles, and the concentrations of Al, Nb and Th for individual samples are listed in Supplementary Table ST1.

Supplementary Table ST3. The composition of the oxyhydroxide and exchangeable phases. The calculated ε_{Nd} values of the residual phases and the ε_{Nd} difference between the parent basalt and residual phases are also given.

Sample code	Depth (cm)	Exchangeable		Oxyhydroxides			Nd_{Res} (%)*	ε_{Nd}^{Res}	$\Delta\varepsilon_{Nd}^{P\text{-}Res}$
		Mn	Nd	Mn	Nd	ε_{Nd}^{ox}			
		µg/g		µg/g					
Dalahi profile (DP)									
RJS 3	32	40.8	0.29	992	0.33	2.57	98	-1.18	2.37
RJS 4	43	16.2	0.18	1138	0.77	3.30	96	-0.65	1.84
RJS 5	53	26.1	0.17	550	0.40	15.3	97	-0.43	1.62
RJS 6	66	14.0	0.16	1115	0.35	9.21	98	-0.94	2.14
RJS 7	78	8.34	0.14	787	0.44	12.2	98	0.18	1.02
RJS 8	87	15.0	0.14	487	0.41	1.17	97	0.20	0.99
RJS 9	99	9.66	0.10	298	0.28	6.32	98	0.62	0.57
RJS 10	110	20.9	0.15	309	0.47	4.95	97	-0.16	1.35
RJS 11	124	22.9	0.14	232	0.24	1.39	98	-0.14	1.33
RJS 12	235	15.2	0.13	388	0.24	9.97	98	0.18	1.01
RJS 13	247	6.38	0.03	19.7	0.46	1.30	96	1.19	0.00
RJS 14	269	1.50	0.03	3.15	0.49	1.49	96	1.88	-0.68
RJS 15	296	2.75	0.02	8.51	0.35	1.38	97	1.33	-0.14
RJS 16 (parent)	376	1.80	0.02	6.91	0.42	1.76	97	1.17	0.02
Pakuria profile (PP)									
PB1	90	4.57	1.00	829	3.75	2.11	84	-1.21	3.66
PB2	125	9.75	0.30	298	2.23	3.70	83	0.15	2.30
PB3	165	2.98	0.48	780	2.21	1.65	88	-1.41	3.87
PB4	225	6.84	0.12	147	3.12	4.45	74	0.85	1.60
PB5	290	5.71	0.13	156	2.60	4.69	80	1.07	1.38
PERN	325	2.46	0.03	82.8	1.64	4.87	86	1.58	0.88
PFAA	625	0.87	0.05	15.1	0.59	4.52	95	2.05	0.40
PFB1 (parent)	1000	6.11	0.03	10.4	0.30	4.78	97	2.39	0.06

*Fraction of Nd in residual weathered phases = $\{(1-[Nd]_{Ox}/[Nd]_{bulk}) \times 100\}$, where ox and bulk represent oxyhydroxide and bulk phases, respectively. $[Nd]_{bulk}$ values are in Supplementary Table ST1

See Supplementary Note SN4 for the determination of ε_{Nd} of residual phase (ε_{Nd}^{Res}).

Supplementary Table ST4. Mean particulate ε_{Nd} values and discharge of global rivers during low and high flow periods.

River Name	Station Name	Length (km)[&]	Average ε_{Nd}				$\Delta\varepsilon_{Nd}^{LQ-HQ}$	±2σ	Average discharge×10^3 (m^3/s)		Discharge contrast (Q_c) (%)[*]	ε_{Nd} and discharge data source
			High discharge		Low discharge				High discharge (HQ)	Low discharge (LQ)		
			ε_{Nd}^{HQ}	±2σ	ε_{Nd}^{LQ}	±2σ						
Time Series Data												
Amazon	Obidos	3869	-11.00	0.07	-10.06	0.09	0.94	0.11	244±12	88±7	64	Rousseau et al. 2019
Orinoco	Ciudad bolivar	1570	-14.17	0.06	-13.72[(i)]	0.05	0.45	0.08	66±4	11±6	84	Rousseau et al. 2019
Maroni	Langa Tabiki	389	-24.87	0.09	-22.80[(ii)]	0.09	2.07	0.13	4.2±0.4	0.9±0.4	78	Rousseau et al. 2019
Solimoes[#]	Manacapuru	1996	-9.39	0.10	-9.09[(i)]	0.06	0.30	0.11	126±1	80±0.3	30	Viers et al. 2008
Madeira[#]	Porto Velho	1869	-12.01[(i)]	0.05	-11.27	0.08	0.74	0.09	24±1	5±2	78	Viers et al. 2008
Tumbes (2007-2008)	El Tigre	182	-6.36	0.12	-3.42	0.07	2.94	0.14	0.117±0.053	0.015±0.002	88	Moquet et al. 2020
Tumbes (2010-2011)	El Tigre	182	-6.30	0.08	-3.45[(ii)]	0.05	2.84	0.09	0.327±0.055	0.026±0.014	92	Moquet et al. 2020
Minjiang	S04	685	-11.82	0.21	-10.71	0.07	1.11	0.23	4.4	0.9±0.8	79	Jian et al. 2020b
Changjiang	Nanjing	4429	-10.96	0.10	-11.79	0.08	-0.84	0.13	44±4	13±2	70	Mao et al. 2011
Seasonal discrete data												
Ganga	Harding bridge	1993	-18.49		-17.95		0.54		41.5	18.0	57	Lupker et al. 2011;2013
Brahmaputra[$]	Guwahati	1974	-12.79		-12.50		0.29		38.5	20.2	48	Singh et al. 2002
Changjiang	Datong	4279	-14.75	0.15	-13.42	0.10	1.33	0.18	62.9	43.3	31	Luo et al. 2012
Parana[$]	Rosario	3580	-10.30	0.18	-11.20	0.18	-0.90	0.25	15.5	12.0	23	Henry et al. 1996
Uruguay[$]	Gualeguaychu	1710	-6.70	0.18	-6.00	0.18	0.70	0.25	7.3	4.6	37	Henry et al. 1996
Amazon[#]	Obidos	3869	-10.30	0.18	-10.12	0.25	0.18	0.31	255	118	54	Merschel et al. 2017
Tapajos[#]	Alter do Chao	2218	-18.79	0.14	-19.33	0.39	-0.55	0.41	10.3	7.6	26	Merschel et al. 2017
Xingu[#]	Porto de Moz	2060	-25.05	0.39	-22.53	0.33	2.52	0.51	5.5	1.8	66	Merschel et al. 2017

[&]River length from the origin, sourced from UNH/GRDC Composite Runoff Fields V1.0.
[*]Discharge contrast (Q_c) = [(HQ-LQ) × 100/HQ].
[#]Discharge data from HyBam research program (http://www.ore-hybam.org).
[$]River water discharge data from UNH/GRDC Composite Runoff Fields V1.0.
[(i)]Two outliers excluded. [(ii)]One outlier excluded.
Calculations of ε_{Nd} and discharge mean for the HQ and LQ periods are explained in Supplementary Note SN6.

Supplementary Table ST5. Results of regression analysis of particulate ε_{Nd} vs. discharge of time series data.

River	Range of ε_{Nd}	r	p	n
Tumbes (2007-2008)	-7.76 to -1.89	-0.71	0.01	11
Tumbes (2010-2011)[$]	-6.70 to -2.42	-0.76	0.01	11
Amazon	-11.41 to -9.77	-0.77	0.003	12
Orinoco[*]	-14.55 to -13.71	-0.65	0.05	9
Maroni[@]	-25.20 to -21.20	-0.76	0.02	9
Madeira[&]	-12.11 to -10.85	-0.66	0.04	10
Solimoes[#]	-9.87 to -8.93	-0.58	0.1	8
Minjiang	-11.8 to -10.2	-0.69	0.01	13
Changjiang	-12.07 to -10.55	0.77	0.002	13

r=correlation coefficient, **p**=confidence limit and **n**=number of data points that were subject to regression.
The outliers excluded from the regression analysis: [$]One outlier of lean flow period. *Two outliers of lean flow period. [@]One outlier each for the lean and peak flow period. [&]Two outliers of peak flow period. [#]Two outliers of lean and one outlier of peak flow period.
Data sources given in Supplementary Table ST4.

Supplementary References

Aydin, O., Yassikaya, M. Y., 2022. Validity and reliability analysis of the PlotDigitizer software program for data extraction from single-case graphs. Perspectives on Behavior Science 45, 239-257. https://doi.org/10.1007%2Fs40614-021-00284-0

Baksi, A. K., 2022. Geochemistry and geochronology of the Rajmahal Flood Basalt Province, northeastern India: Genetic links to Kerguelen hotspot activity. Journal of Earth System Science 131, 157. https://doi.org/10.1007/s12040-022-01855-8

Bhattacharyya, R., Singh, S. P., Qasim, A., Chandrashekhar, A. K., 2024. Geochemical and radiogenic Sr-Nd isotope characterization of widespread sandy surface sediments in the Great Indian Desert, Thar: Implications for provenance studies. Journal of Geophysical Research: Earth Surface 129(8), e2023JF007625. https://doi.org/10.1029/2023JF007625

Chatterjee, J., Singh S. K., 2014. Dissolved Nd in the Ganga River system and its flux to the Bay of Bengal, Goldschmidt. https://goldschmidtabstracts.info/2014/387.pdf

Chauvel, C., Garçon, M., Bureau, S., Besnault, A., Jahn, B. M., Ding, Z., 2014. Constraints from loess on the Hf–Nd isotopic composition of the upper continental crust. Earth and Planetary Science Letters, 388 48-58. https://doi.org/10.1016/j.epsl.2013.11.045

Galy, A., France-Lanord, C., Hurtrez, J. E., 1998. Distribution of physical erosion in Himalaya from river particle geochemistry. Mineralogical Magazine 62, 493-494. http://dx.doi.org/10.1180/minmag.1998.62A.1.261

Ghose, N. C., Chatterjee, N., Windley, B. F., 2017. Subaqueous Eruptive Phase of the Late Aaptian Rajmahal Volcanism India: Evidence from Volcaniclastic Rocks, Bentonite, Black Shales and Oolite. Geoscience Frontiers 8, 809-822. https://doi.org/10.1016/j.gsf.2016.06.007

Ghosh, S., Guchhait, S. K., 2015 Characterization and evolution of primary and secondary laterites in northwestern Bengal Basin, West Bengal, India. Journal of Palaeogeography 4, 203-230. https://doi.org/10.3724/SP.J.1261.2015.00074

Ghosh, S., Guchhait, S. K., 2019. Modes of formation, palaeogene to early quaternary palaeogenesis and geochronology of laterites in rajmahal basalt traps and Rarh Bengal of Lower Ganga Basin. Quaternary Geomorphology in India: Case Studies from the Lower Ganga Basin, 25-60. https://doi.org/10.1007/978-3-319-90427-6_2

Henry, F., Probst, J. L., Thouron, D., Depetris, P., Garçon, V., 1996. Nd-Sr isotopic compositions of dissolved and particulate material transported by the Parana and Uruguay rivers during high (December 1993) and low (September 1994) water periods. Geological Sciences, Bulletins and Memoirs 49, 89-100.

Hindshaw, R. S., Aciego, S. M., Piotrowski, A. M., Tipper, E. T., 2018b. Decoupling of dissolved and bedrock neodymium isotopes during sedimentary cycling. Geochemical Perspectives Letters 8, 43-46. https://doi.org/10.7185/geochemlet.1828

Hindshaw, R. S., Tosca, N. J., Piotrowski, A. M., Tipper, E. T., 2018a. Clay mineralogy, strontium and neodymium isotope ratios in the sediments of two High Arctic catchments (Svalbard). Earth Surface Dynamics 6, 141-161. https://doi.org/10.5194/esurf-6-141-2018

Jacobsen, S. B., Wasserburg, G. J., 1980. Sm-Nd isotopic evolution of chondrites. Earth and Planetary Science Letters 50, 139-155. https://doi.org/10.1016/0012-821X(80)90125-9

Jian, X., Yang, S., Hong, D., Liang, H., Zhang, S., Fu, H., Zhang, W., 2020a. Seasonal geochemical heterogeneity of sediments from a subtropical mountainous river in SE China. Marine Geology 422, 106120. https://doi.org/10.1016/j.margeo.2020.106120

Jian, X., Zhang, W., Yang, S., Kao, S. J., 2020b. Climate-dependent sediment composition and transport of mountainous rivers in tectonically stable, subtropical East Asia. Geophysical Research Letters 47, e2019GL086150. https://doi.org/10.1029/2019GL086150

Larkin, C.S., Piotrowski, A.M., Hindshaw, R.S., Bayon, G., Hilton, R.G., Baronas, J.J., Dellinger, M., Wang, R., Tipper, E.T., 2021. Constraints on the source of reactive phases in sediment from a major Arctic River using neodymium isotopes. Earth and Planetary Science Letters 565, p.116933.https://doi.org/10.1016/j.epsl.2021.116933

Luo, C., Zheng, H., Wu, W., Wang, P., Chen, Y., Wei, X., 2012. Sr-Nd isotope stratification along water depth: An example from Datong hydrological station of Yangtze River. Chinese Science Bulletin 57, 4482-4490. https://doi.org/10.1007/s11434-012-5311-z

Lupker, M., France-Lanord, C., Galy, V., Lavé, J., Kudrass, H., 2013. Increasing chemical weathering in the Himalayan system since the Last Glacial Maximum. Earth and Planetary Science Letters 365, 243-252. https://doi.org/10.1016/j.epsl.2013.01.038

Lupker, M., France-Lanord, C., Lavé, J., Bouchez, J., Galy, V., Métivier, F., Gaillardet, J., Lartiges, B., Mugnier, J. L., 2011. A Rouse-based method to integrate the chemical composition of river sediments: Application to the Ganga basin. Journal of Geophysical Research: Earth Surface, 116(F4). https://doi.org/10.1029/2010JF001947

Ma, J. L., Wei, G. J., Xu, Y. G., Long, W. G., Sun, W. D., 2007. Mobilization and re-distribution of major and trace elements during extreme weathering of basalt in Hainan Island, South China. Geochimica et Cosmochimica Acta 71(13), 3223-3237. https://doi.org/10.1016/j.gca.2007.03.035

Mao, C., Chen, J., Yuan, X., Yang, Z., Balsam, W., Ji, J., 2010. Seasonal variation in the mineralogy of the suspended particulate matter of the lower Changjiang River at Nanjing, China. Clays and Clay Minerals 58, 691-706. https://doi.org/10.1346/CCMN.2010.0580508

Mao, C., Chen, J., Yuan, X., Yang, Z., Ji, J., 2011. Seasonal variations in the Sr-Nd isotopic compositions of suspended particulate matter in the lower Changjiang River: Provenance and erosion constraints. Chinese Science Bulletin 56, 2371-2378. https://doi.org/10.1007/s11434-011-4589-6

Maynard, J. B., 1992. Chemistry of modern soils as a guide to interpreting Precambrian paleosols. The Journal of Geology 100, 279-289. https://doi.org/10.1086/629632

Merschel, G., Bau, M., Schmidt, K., Münker, C., Dantas, E. L., 2017. Hafnium and neodymium isotopes and REY distribution in the truly dissolved, nanoparticulate/colloidal and suspended loads of rivers in the Amazon Basin, Brazil. Geochimica et Cosmochimica Acta 213, 383-399. https://doi.org/10.1016/j.gca.2017.07.006

Moquet, J.S., Morera, S., Turcq, B., Poitrasson, F., Roddaz, M., Moreira-Turcq, P., Espinoza, J.C., Guyot, J.L., Takahashi, K., Orrillo-Vigo, J., Petrick, S., Mounic, S., Sondag, F., 2020. Control of seasonal and inter-annual rainfall distribution on the Strontium-Neodymium isotopic compositions of suspended particulate matter and implications for tracing ENSO events in the Pacific coast (Tumbes basin, Peru). Global and Planetary Change 185, 103080. https://doi.org/10.1016/j.gloplacha.2019.103080

Mukherjee, P. K., 1971. Petrology of Rajmahal Traps of the NW Rajmahal Hills, India. Bulletin of Volcanology 35, 887-906. https://doi.org/10.1007/BF02596853

Nesbitt, H. W., Markovics, G., 1997. Weathering of granodioritic crust, long-term storage of elements in weathering profiles, and petrogenesis of siliciclastic sediments. Geochimica et Cosmochimica Acta 61, 1653-1670. https://doi.org/10.1016/S0016-7037(97)00031-8

Rousseau, T. C., Roddaz, M., Moquet, J. S., Delgado, H. H., Calves, G., Bayon, G., 2019. Controls on the geochemistry of suspended sediments from large tropical South American rivers (Amazon, Orinoco and Maroni). Chemical Geology 522, 38-54. https://doi.org/10.1016/j.chemgeo.2019.05.027

Singh, S. K., France-Lanord, C., 2002. Tracing the distribution of erosion in the Brahmaputra watershed from isotopic compositions of stream sediments. Earth and Planetary Science Letters 202, 645-662. https://doi.org/10.1016/S0012-821X(02)00822-1

Tachambalath, A. P., France-Lanord, C., Galy, A., Rigaudier, T., Charreau, J., 2023. Data report: major and trace element composition of silicates and carbonates from Bengal Fan sediments, IODP Expedition 354. https://doi.org/10.14379/iodp.proc.354.204.2023

Taylor, S.R., McLennan, S.M., 1985. The Continental Crust: Its Composition and Evolution. Blackwell, Oxford, UK, 349.

Tricca, A., Stille, P., Steinmann, M., Kiefel, B., Samuel, J., Eikenberg, J., 1999. Rare earth elements and Sr and Nd isotopic compositions of dissolved and suspended loads from small river systems in the Vosges mountains (France), the river Rhine and groundwater. Chemical Geology 160, 139-158. https://doi.org/10.1016/S0009-2541(99)00065-0

Viers, J., Roddaz, M., Filizola, N., Guyot, J.L., Sondag, F., Brunet, P., Zouiten, C., Boucayrand, C., Martin, F., Boaventura, G.R., 2008. Seasonal and provenance controls on Nd–Sr isotopic compositions of Amazon rivers suspended sediments and implications for Nd and Sr fluxes exported to the Atlantic Ocean. Earth and Planetary Science Letters 274, 511-523. https://doi.org/10.1016/j.epsl.2008.08.011

Wang, Z., Ma, J., Li, J., Wei, G., Zeng, T., Li, L., Zhang, L., Deng, W., Xie, L., Liu, Z., 2018. Fe (hydro) oxide controls Mo isotope fractionation during the weathering of granite. Geochimica et Cosmochimica Acta, 226 1-17. https://doi.org/10.1016/j.gca.2018.01.032

Yuan, W., Gong, Y., Chen, J., Wang, Z., Huang, F., Yang, X., Chetelat, B., Teng, H., Schott, J., 2022. Gallium isotope constraints on the intense weathering of basalt. Geochimica et Cosmochimica Acta, 333 22-38. https://doi.org/10.1016/j.gca.2022.06.042